INTERACTION STUDY OF GLASS SEALENTS AND ELECTROLYTE OF SOLID OXIDE FUEL CELL

Thesis submitted in partial fulfillment of the requirement for
The award of the degree of

Master of Technology (M. Tech.)
In
MATERIALS SCIENCE AND ENGINEERING

Submitted By

SARITA DEVI SHARMA
Roll No.60602014

Under the guidance of

Dr. KULVIR SINGH
Assistant Professor

School of Physics & Material Sciences
Thapar University, Patiala
Patiala - 147001
June-2008

Dedicated to my Loving Family

CERTIFICATE

This is to certify that Ms. SARITA DEVI SHARMA, Roll No. 6060201[illegible]4 has worked on the thesis entitled "INRERACTION STUDY OF GLASS SEALANTS AND ELECTROLYTE FOR SOLID OXIDE FUEL CELL" in the partial fulfillment for award of the degree of MASTERS OF TECHNOLGY in Material Science and Engineering. I certify that the matter embodied in this report is of the candidate's own record and not submitted to any other university in any part or full form for the award of such kind of a degree.

(Dr. KULVIR SINGH)
Supervisor
SPMS, Thapar University
Patiala

Countersigned by:

Dr.O.P.Pandey
(Prof. & Head)
School of Physics and Materials Science
Thapar University, Patiala

Dr. R.K.Sharma
Dean of academic Affairs
Thapar University,
Patiala

ACKNOWLEDGEMENT

No matter how much enterprising and entrepreneurial one's thinking is, yet nobody can do everything all by himself without some help and guidance. It is inhumane if the concerned person's assistance goes without appreciation and thanks. My first and foremost offering of thanks goes to my guide and mentor **Dr. Kulvir Singh**. Perseverance, exuberance, positive approaches are just some of the traits he imprinted on my personality. I thank him from the core of my heart for his invaluable advice, positive criticism, stimulating discussion and consistent encouragement. His meticulous attention towards my proceedings, his devoted time and his ideas has enabled me to make the project a success. His faith in me has always made me more confident. It had been my privilege to work under his guidance.

I am grateful to **Dr. O.P. Pandey, Prof. and Head, School of Physics and Material Science, Thapar University, Patiala** for encouragement and execution of thesis work.

Various factors, situations and persons integrate to provide the background for the accomplishment of a task. Foremost, I'm indebted to **God** almighty that has been there today and always.

My special thanks to P G Lab incharge **Mr. Purushottam** for his help to carry out X-Ray diffraction study. I would also like to thank **Mr. Jant Singh**, for providing all kind of assistance in PG Lab for creating a healthy research environment.

It gives me immense pleasure to express my special thank to Research Scholar **Mr. Vishal Kumar** for his assistance, cooperation and valuable suggestions. He has helped me a lot at various stages during the due course of my thesis work.

I would also like to give many thanks to Research Scholars **Kamal, Shefali, Anu, Zinki, Jasmeet and Akshay** for their valuable suggestions and help.

I am grateful to all my friends specially **Indu, Vishal, Ravinder, Alok, Sanjay** and **Yousuf** for their support and cooperation.

All the faculties and my colleagues at the SPMS are acknowledged for providing me a friendly atmosphere and encouraging me throughout this research.

Last but not the least; I would like to thank my family for their moral support that kept my spirit up during the endeavor.

Sarita Sharma

Sarita Devi Sharma

Roll No. 60602014

ABSTRACT

The chemical interactions between different $SrO\text{-}SiO_2\text{-}B_2O_3\text{-}A_2O_3$ {A= Y, La, Al and Cr) based glass sealants and $Bi_4V_{1.8}Al_{0.2}O_{11}$ electrolyte are investigated. The glass and electrolyte are taken in 3:1 wt% respectively. Mixture of these components were heat treated for different time durations and then characterized by X-Ray diffraction (XRD), Fourier Transform Infra Red spectroscopy (FTIR) and dilatometer, to determine the possible reaction phases their volume fraction and prominent band formation. During heat treatment main phases formed were $SrVSi_2O_7$, $AlVO_4$, YVO_4, Cr_2SiO_4. The volume fraction of the various phases depends on the Al_2O_3, Y_2O_3, Y_2O_3 and Cr2O3 along with heat treatment durations. The FTIR spectra of all the samples exhibit three bands i ,e 400-600 cm^{-1}, 650-800 cm^{-1} and 800- 1300 cm^{-1} . These spectra are assigned to bending vibrations of the Si-0-Si linkages, bending vibrations of the A-O (A= Y, La, Al and Cr) bonds and stretching vibrations of the SiO_4 tetrahedron with the different numbers of bridging oxygen atoms. The thermal expansion coefficient of diffusion couple is 8X 10^{-6}/°C which is very close to desired value of SOFC.

CONTENTS

LIST OF TABLES

LIST OF FIGURES

LIST OF ABBREVIATIONS

SOFC	Solid Oxide Fuel Cell

PAFC	Phosphoric Acid Fuel Cell
AFC	Alkaline Fuel Cell
PEMFC	Proton Exchange Membrane Fuel Cell
DMFC	Direct Methanol Fuel Cell
MCFC	Molten Carbonate Fuel Cell
XRD	X-Ray Diffraction
FTIR	Fourier Transform Infra Red
TEC	Thermal Expansion Coefficient
YSZ	Yttria stabilized Zirconia

CHAPTER-1

INTRODUCTION

1.1 Fuel cell

The modern scientific and technological approach, in the area of energy production is to develop inexpensive devices, which could satisfy the current drive for cleaner and more efficiently distributed power, particularly in combination of heat and power systems. In this context, fuel cells represent a promising and viable alternative for large scale generation of electricity, with minimal undesirable chemical, thermal and acoustic emissions. A fuel cell is a device that directly converts the chemical energy of reactants (a fuel such as hydrogen, natural gas, methane or methanol and oxygen), into electricity. Fuel cells are currently attracting tremendous interest because of their huge potential for power generation in stationary, portable and transport applications and our increasing need for sustainable energy resources. The combination of the high efficiency with which chemical energy is converted directly into electrical energy, and the very much lower emissions of sulfur and nitrogen oxides and hydrocarbon pollutants, and significantly reduced CO_2 emissions, confers very significant environmental advantages on fuel cells over conventional power generation. However, significant advances in the development of both materials with improved properties and in manufacturing processes in the last two decades have made fuel cells a realistic proposition to compete on a commercial footing with conventional power generation.

The concept of the fuel cell was first demonstrated in 1839 by William Grove [1]. While investigating the electrolysis of water, Grove observed that when the current was switched off, a small current flowed through the circuit in the opposite direction, as a result of a reaction between the electrolysis products, hydrogen and oxygen, catalyzed by the platinum electrodes. Ceramic fuel cells came into existence much later and began with Nernest's discovery of solid-oxide electrolytes in 1899 and the operation of the first ceramic fuel cell at a temperature of 1000°C was demonstrated by Baur and Pries in 1937. In their experiment they used zirconium, yttrium, cerium, lanthanum and tungsten as electrolytes, with little success. Much of the research, however, was short-lived as melting, short circuiting, and high electrical resistance inside the cell materials created numerous technical hurdles. Their designs were not as good to provide electrical conductivity up to the mark as was expected due to unwanted chemical reactions between the electrolytes and various gases, including carbon monoxide. By the late

1950's, research into solid oxide technology began to accelerate because of advancement in ceramic processing.

1.2 Types of fuel cells

Fuel cells are classified primarily by the kind of electrolyte they employ. This determines the kind of chemical reactions that take place in the cell, the kind of catalysts required, the temperature range in which the cell operates, the fuel required, and other factors. These characteristics, in turn, affect the applications for which these cells are most suitable. There are several types of fuel cells currently under development, each with its own advantages, limitations, and potential applications. The main focus of research on fuel cells is now to improve fuel cell behavior with regard to:

- Lifetime,
- Operating temperatures,
- Catalytic or conductivity efficiencies,
- Or simply manufacturing issues by using different materials in electrodes and electrolytes.

.

Based on the type of electrolyte used fuel cells can be categorized as:-

(1)Phosphoric Acid Fuel Cell (PAFC)

(2)Alkaline Fuel Cell (AFC)

(3)Proton Exchange Membrane Fuel Cell (PEMFC)

(4)Direct Methanol Fuel Cell (DMFC)

(5)Molten Carbonate Fuel Cell (MCFC)

(6)Solid Oxide Fuel Cell (SOFC)

1.2.1 Phosphoric Acid Fuel Cell (PAFC)

Phosphoric acid fuel cells use liquid phosphoric acid as an electrolyte—the acid is contained in a Teflon-bonded silicon carbide matrix—and porous carbon electrodes containing a platinum catalyst [4]. The phosphoric acid fuel cell (PAFC) is considered the "first generation" of modern fuel cells. It is one of the most mature cell and the first to be used commercially. This type of fuel cell is typically used for stationary power generation, but some PAFCs have been used to power large vehicles such as city buses. One of the main advantages to this type of fuel cell is that it can use impure hydrogen as fuel.

Disadvantages of PAFCs include: it uses expensive platinum as a catalyst, it generates low current and power comparably to other types of fuel cells, and it generally has a large size and weight. PAFCs, however, are the most mature fuel cell technology.

1.2.2 Alkaline Fuel Cell (AFC)

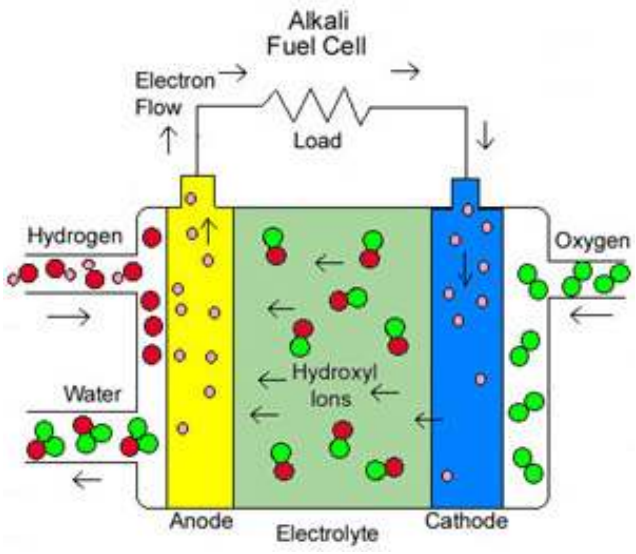

Fig 1.1: Diagrammatic Representation of AFC

Long used by NASA on space missions, these cells can achieve power generating efficiencies of up to 70 %. They were used on the Apollo spacecraft to provide both electricity and drinking water [4]. Their operating temperature is 150 to 200°C. They used an aqueous solution of alkaline potassium hydroxide soaked in a matrix as the electrolyte shown in fig 1.1. The big advantages of this system are its very short start-up time, less use of expensive materials and high efficiencies compared to the other fuel cell types [5]. Until recently they were too costly for commercial applications. They typically have a cell output from 300 watts to 5 kW. AFCs' high performance is due to the rate at which chemical reactions take place in the cell. They have also demonstrated efficiencies near 60 % in space applications.

The main disadvantage of the AFC is probably its sensitivity of the potassium hydroxide to CO_2-poisoning and of the catalyst to CO-poisoning [5]. In fact, even the small amount of CO_2 in the air can affect this cell's operation, making it necessary to purify both the hydrogen and oxygen used in the cell.

1.2.3 Proton Exchange Membrane Fuel Cell (PEM)

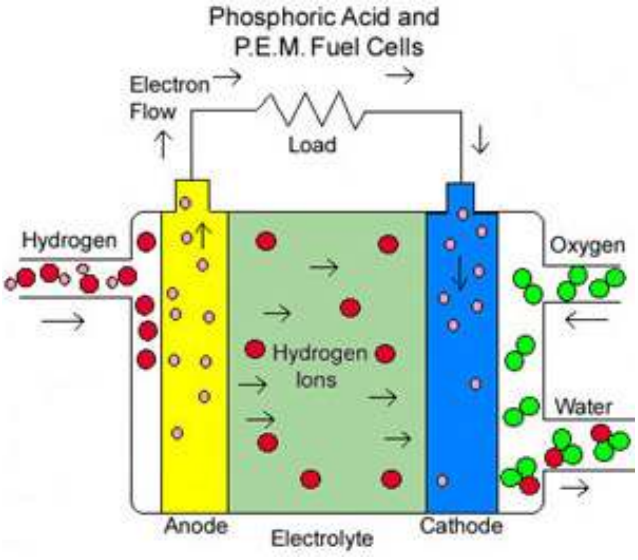

Fig 1.2: Diagrammatic Representation of PEM

Polymer electrolyte membrane (PEM) fuel cells—also called proton exchange membrane fuel cells—deliver high power density and offer the advantages of low weight and volume, compared to other fuel cells [4,5]. The simple working of the fuel cell is shown in fig 1.2. PEM fuel cells use a solid polymer as an electrolyte and porous carbon electrodes containing a platinum catalyst. This solid electrolyte allows a compact construction of the fuel cell and also allows more straightforward operation under pressure, which can improve the performance considerably. They need only hydrogen, oxygen from the air, and water to operate and do not require corrosive fluids like some fuel cells. These cells operate at relatively low temperatures about 80°C have high power density, can vary their output quickly to meet shifts in power demand, and are suited for various applications, such as in automobiles due to quick startup is required.

This type of fuel cell is, however, sensitive to fuel impurities. Cell outputs generally range from 50 to 250 kW. The drawback of the use of platinum is the fact that CO concentration of even 10 ppm causes performance degradation of the cells [5]. However, the combination of Platinum/Ruthenium in the electro-catalyst, improves the tolerance.

1.2.4 Direct Methanol Fuel Cells (DMFC)

Most fuel cells are powered by hydrogen, which can be fed to the fuel cell system directly or can be generated within the fuel cell system by reforming hydrogen-rich fuels such as methanol, ethanol, and hydrocarbon fuels [4, 5]. Direct methanol fuel cells (DMFCs), however, are powered by pure methanol, which is mixed with steam and fed directly to the fuel cell anode. Methanol undergoes electrochemical reaction with water to CO2 at an operating temperature of 80 to 130°C. This low temperature makes short startup time possible. Efficiencies of about 40% are expected with this type of fuel cell, which would typically operate at a temperature between 50 -100 °C. This is a relatively low range, making this fuel cell attractive for small to medium-

sized applications, to power cellular phones and laptops. Higher efficiencies are achieved at higher temperatures.

A major problem, however, is fuel crossing over from the anode to the cathode without producing electricity. Other drawbacks of the DMFC are the excessive use of expensive materials like platinum (up to ten times more than high performance PEMFCs) and ruthenium, and the toxicity of CH_3OH. Low cell voltage, resulting in low current density, is caused by cross-over of neutral methanol from anode to cathode side.

1.2.5 Carbonate Fuel Cell (CFC)

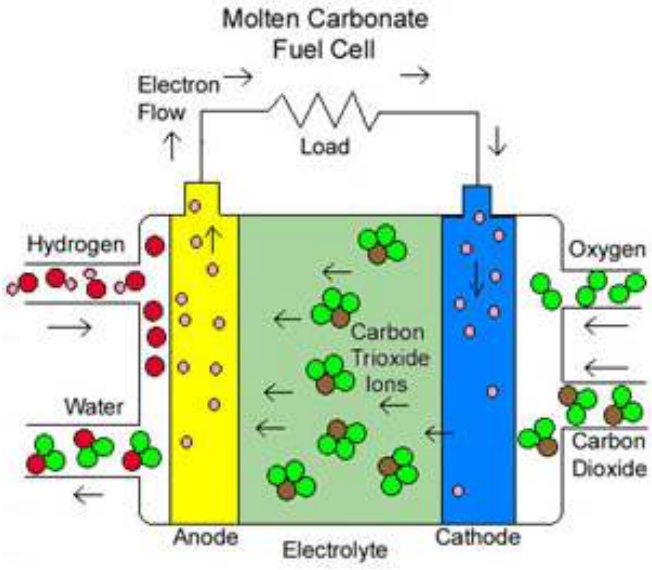

Fig 1.3: Diagrammatic Representation of MCFC

Molten Carbonate fuel cells (MCFC) use high-temperature compounds of salt (like sodium or magnesium) carbonates (chemically, CO_3^{2-} as the electrolyte. Efficiency ranges from 60 to 80 percent, and operating temperature is about 650°C [4, 5]. The high operating temperature serves as a big advantage because this implies higher efficiency and the flexibility to use more types of

fuels and inexpensive catalysts as the reactions involving breaking of carbon bonds in larger hydrocarbon fuels occur much faster as the temperature is increased. The simple diagram of DMFC is shown in fig 1.3. A disadvantage to this, however, is that high temperatures enhance corrosion, the breakdown of cell components and slow start up times.

1.2.6 Solid Oxide Fuel Cell (SOFC)

Solid oxide fuel cell is another highly promising fuel cell; this type could be used in high power applications including industrial and large-scale central electricity generating stations. Some developers also see SOFC use in motor vehicles and are developing fuel cell auxiliary power units (APUs) with SOFCs [4, 6].

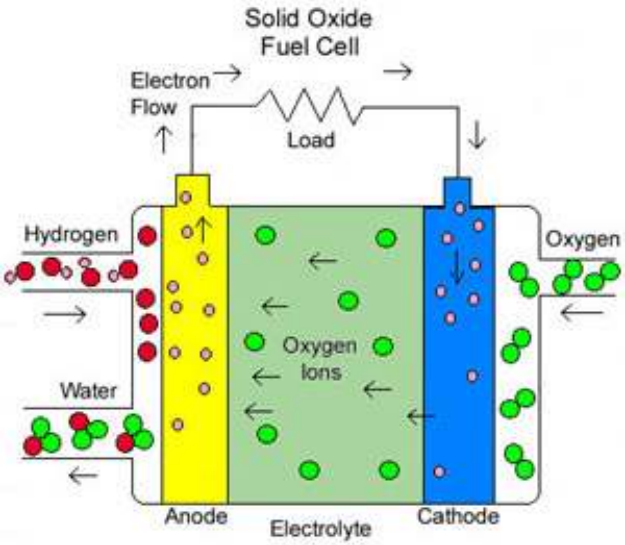

Fig 1.4: Diagrammatic representation of SOFC

In solid oxide fuel system ceramic material such as of solid zirconium oxide and a small amount of yttria is used instead of a liquid electrolyte, allowing operating temperatures to reach 1000°C. Power generating efficiencies could reach 60% and 85% with cogeneration and cell output is up to 100 kW. One type of SOFC uses an array of meter-long tubes (tubular design), and other variations include a compressed disc planar design. Tubular SOFC designs are closer to

commercialization and are being produced by several companies around the world such as Siemens Westinghouse Cooperation, Allied Signal etc. Because SOFCs operate at high temperatures, and therefore lend themselves to applications in which this high-temperature thermal energy can be used. This heat can be used in two basic ways – for heating processes such as that in industry or for integration with turbines for additional electricity production. Working of the SOFC is shown in fig 1.4.

1.3 Advantages of solid oxide fuel cells

The solid oxide fuel cell (SOFC) represents a solid-state; high-temperature (600-1000°C) system eliminates many of the technical challenges, although different limitations arise. In general, a SOFC system is well suited for applications where a high operating temperature and a longer startup transient are not a limitation, or high amounts of CO impurities are present. The main advantages of the SOFC system include [7]:

1) Tolerance to CO, because it is oxidized as a fuel, eliminating one of the main drawbacks of the PEM fuel cell.

2) High operating temperature greatly reduces activation polarization and eliminates the need for expensive catalysts.

3) Potential for internal reformation of hydrocarbons.

4) Potential for high hybrid system efficiencies (~80%).

5) Tolerance to a variety of fuel stocks.

6) High-quality waste heat generated is ideal for a cogeneration system.

Previously mentioned fuel cells and their components, working temperature and applications are summarized in table 1:

Table 1.1**:** Technical details of various fuel cells:-

Fuel Cells	**Temp. Range**	**electrolyte**	**Application**
Polymer Electrolyte Membrane [PEMFC]	Room Temp. to 80°C	polymer	Small Units, up to automobiles
Alkaline Fuel Cell System [AFC]	Room Temp. to 80°C	NaOH or KOH	Small Units, up to automobiles
Phosphoric Acid Fuel Cell [PAFC]	210 to 220°C	H_3PO_4	Power Plants 50 to 200 kW
Molten Carbonate Fuel Cell [MCFC]	620 to 660 °C	$KLiCO_3$	Power Plants up to Mega-Watt
Solid Oxide Fuel Cell Systems [SOFC]	800 to 1000 °C	ZrO_2 with Y_2O_3	Small to Large Power Plants

CHAPTER-2

SOFC AND ITS COMPONENTS

As mentioned in chapter-1, the solid oxide fuel cell (SOFC) has some advantages over other fuel cells. In this chapter more details of SOFC, their designs, components and working are given in details.

2.1 Working of SOFC

The SOFC is constructed with two porous electrodes which sandwich an electrolyte [1]. Air flows along the cathode (which is therefore also called the "air electrode"). When an oxygen molecule contacts the cathode/electrolyte interface, it catalytically acquires electrons from the cathode and splits into oxygen ions. The oxygen ions diffuse into the electrolyte material and migrate to the other side of the cell where they encounter the anode (also called the "fuel electrode"). The oxygen ions encounter the fuel at the anode/electrolyte interface and react catalytically, giving off water vapors, carbon dioxide, heat, and -- most importantly -- electrons. The electrons transport through the anode to the external circuit and back to the cathode, providing a source of useful electrical energy in an external circuit as shown in fig 2.1

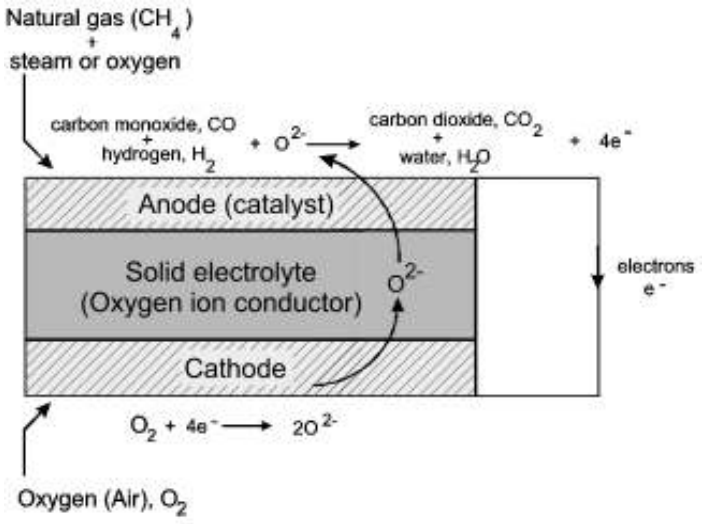

Fig 2.1:- Working of solid oxide fuel cell

2.2 SOFC Design Concepts

To date, there are essentially four different basic designs for the SOFC system i, e the planar, seal-less tubular, monolithic, and segmented cell-in-series design. The monolithic and segmented cell-in-series designs are less developed, although demonstration units have been constructed and operated. The two main types of designs are discussed in the following sections.

2.2.1 Planar design

The most straightforward type of design for a fuel cell is the planar design as shown in figure 2.2. These flat structures allow for a good stack ability of the cells and simple electrical connections between electrodes. Compact stacks thus have minimal ohmic losses and a high power density as compared to other designs of SOFCs.

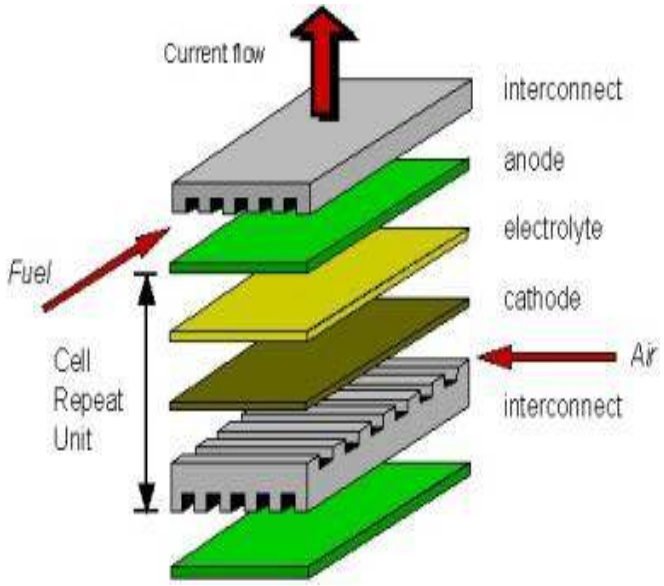

Fig 2.2:-Configuration for a planar design SOFC

However, the planar design has the major drawback of necessitating a sealing agent to prevent gases from leaking and let them properly flow in their respective channels [6, 7]. Compressive, glass, cermets, and glass-ceramic seals have been used. Sealing is still a key issue in planar SOFC design, because it is difficult to maintain system integrity over the large thermal

variation and reducing/oxidizing environment. Other disadvantages are the extreme brittleness in tension of the system, as the tensile strength of typical planar cells is 20% of their compressive strength, but also the possibility that the failure of one single cell may result in the failure of the whole stack**.** Thermal cycling and thermal stresses are also a major issue, due to the thinness of the materials used, which leads to research on temperature variations while the fuel cell is in operation State of the art planar SOFCs use a thick anode as a support for a thin film electrolyte, which allows for a robust yet simple and compact design.

2.2.2 Tabular design

The second design, and probably the most advanced, is the seal-less tubular concept pioneered by Westinghouse (now Siemens-Westinghouse) state. The major advantage of this design is that the problematic high-temperature seals needed for other SOFC designs are eliminated. Tubular designs have been tested in 100 kW atmospheric pressure and 250 kW pressurized demonstration systems with little performance degradation with time. The tubular design of SOFC is given in figure 2.3.

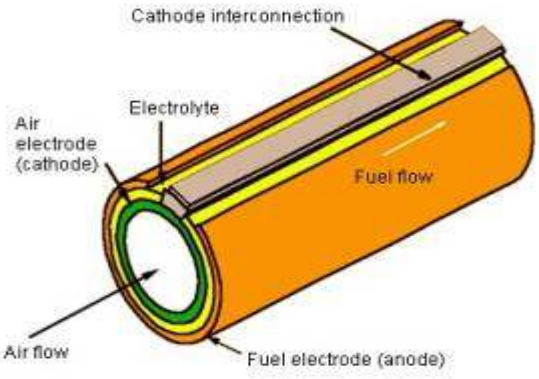

Fig 2.3:- Configuration for a tubular design SOFC

One drawback of this type of tubular design is the more complex and limited range of cell fabrication methods [6, 7]. Another drawback is high internal ohmic losses relative to the planar design, due to the in-plane path that electrons must travel along the electrodes to and from the

cell interconnect. This design can also experience significant losses due to limited oxygen transport through the porous (~35% porosity) structural support tube used to provide rigidity to the assembly. The most obvious one is the high production cost, as the process to fabricate a cylindrical tube of zirconia and to deposit metals on both sides, chemical vapor deposition (CVD) is carried out in a vacuum chamber.

2.3 Material Processing and Selections

The materials for different cell components have been selected based on the following criteria [10]:

(a) Suitable electrical conducting properties required of different cell components to perform their intended cell functions.

(b) Adequate chemical and structural stability at high temperatures during cell operation as well as during cell fabrication.

(c) Minimal reactivity and inter diffusion among different cell components.

(d) Matching thermal expansion among different cell components.

2.3.1 Cathode (Air electrode)

The air electrode operates in an oxidizing environment of air or oxygen at 1000°C and participates in the oxygen reduction reaction. The air electrode in solid oxide fuel cells has to meet the following requirements [8, 10].

(a) High electronic conductivity.

b) Chemical and dimensional stability in environments encountered during cell operation and during fabrication of interconnection, electrolyte and fuel electrode layers.

(c) Thermal expansion matches with other cell components.

(d) Compatibility and minimum reactivity with the electrolyte and the interconnection with which air electrode comes into contact.

(e) Sufficient porosity to facilitate transport of molecular oxygen from the gas phase to the air electrode / electrolyte interface.

Cathodes are generally made of lanthanum compounds. $LaMnO_3$ is a p-doped perovskite structure which can undergo atomic distortion changing the shape of unit cells [6, 9]. It can easily acquire excesses or deficiencies in either Lanthanum or Oxygen, making it easy to match the substrate crystalline structure. However particular attention must be given to temperature variations as they are a major factor in the appearance of those defects. $LaMnO_3$ has intrinsic cation vacancies resulting in its p-type nature. Its conductivity can be further enhanced by replacing some atoms with lower- valence cations such as strontium, barium, nickel, magnesium or calcium. Strontium has currently proved to be the best dopant under oxidizing conditions. The substitution of La^{3+} with Sr^{2+} allow for a higher concentration of Mn^{4+} ions favoring conductivity. Furthermore, the reactivity and inter diffusion studies between doped lanthanum manganite and yttria stabilized zirconia electrolyte have shown any interactions between these two materials at 1000°C to be minimal. Other materials of the same class as $LaMnO_3$ are investigated, such as $LaCoO_3$, which has large oxygen deficiencies at high temperatures. This particular compound has a better conductivity under similar conditions, but is much less stable against reduction reactions. Tin-doped Indium Oxide has also been considered but was deemed too costly. For SOFC substantially operating at lower temperature, such as 600-800 ° C, alternative cathode material has been developed and optimized since LaMnO3 does not appear to be a satisfactory choice at lower temperature, owing to its low ionic conductivity and slower oxygen transfer kinetics. For these cases other pervoskite structure materials such as containing Co, Fe or Ni has received greater attraction but there are certain limitations such as TEC mismatching of Co with electrolyte, and electrical conductivity of Fe is low but promising results has been obtained by using these materials.

2.3.2 Anode (Fuel electrode)

The requirements for the fuel electrode are similar to that of cathode [7, 10]. The main function of the anode is to facilitate the adsorption and oxidation of hydrogen from the fuel stream, thus permitting the oxygen ions from the electrolyte to combine with the hydrogen to form water and release electrons to the external circuit. One popular and very cheap material used as an anode for SOFCs is a Nickel-YSZ cermets, where the excellent electrical conductivity of nickel is combined with a porous YSZ powder and sintered at 1400°C, resulting in a highly porous, conductive electrode with many three-phase contact points. Nickel however, tends to catalyze the formation of carbon filaments in the absence of added steam and Ni-YSZ cermets are thus not an optimal choice in SOFCs where the use of carbon-based gases is often considered [13]. There is a thermal expansion coefficient mismatch between nickel and YSZ causing cracks in either the electrode or the electrolyte material. Copper and cobalt are two other materials that are beginning to see a wider use in fuel cell anodes. Although copper, and cobalt even more so, are more expensive than nickel they still are a better compromise than platinum. These metals can also withstand the high temperatures of a SOFC without being oxidized. Copper-ceria cermets anode has been studied for the direct oxidation of hydrocarbon fuels. Copper suppresses carbon formation during direct oxidation while ceria improves the reaction kinetics. Unlike nickel, copper does not catalyze the carbon formation. If proven adequate for moderate to high power density operation, the direct oxidation scheme for fuel utilization in SOFC can potentially eliminate external or integral reforming of fuels.

2.3.3 Inter connector or separator

Interconnection serves as the electric contact to the air electrode and also protects the air electrode material from the reducing environment of the fuel on the fuel electrode side. The requirements of the interconnecter are [8, 10] -

(a) Nearly 100% electronic conductivity.

(b) Stability in both oxidizing and reducing atmospheres at the cell operating temperature.

(c) Low permeability for oxygen and hydrogen to minimize direct combination of oxidant and fuel during cell operation.

(d) A thermal expansion close to that of the air electrode and the electrolyte.

(e) Non-reactivity with the electrodes, and easy to be fabricated.

(f) Low volatility and moderate cost.

Cell interconnects provide cell-to-cell electrical connection and separate fuel and oxidant gas atmospheres in a cell stack. Two classes of SOFC interconnect materials have been extensively used in high-temperature and intermediate-temperature SOFCs, electronically conducting perovskite chromite ceramics, and metallic alloys.

Doped lanthanum chromite ($LaCrO_3$) ceramic is currently the most common candidate material for SOFCs for cells operating at temperature above 800°C and in $LaCrO_3$ oxide based solid solutions, Sr, Ca, Mg, Ni, or other elements are doped. Lanthanum chromite is a p-type conductor; its conductivity is due to small polaron hopping from room temperature to 1400°C at oxygen pressures as low as 10^{-18} atm. The conductivity is enhanced as lower valence ions (e.g. Ca, Mg, Sr, etc.) are substituted on either the La^{3+} or the Cr^{3+} sites [10]. Chromite interconnects suffer from processing difficulties and high cost (high-temperature sintering, reactive powder synthesis, liquid phase additives, etc.).

As an alternative to ceramic interconnects, corrosion-tolerant conductive oxide scale forming commercial and experimental metallic alloys are also currently being investigated for use as current collectors in intermediate-temperature SOFCs. Metals and alloys offer the potential for lower cost, ease of fabrication and joining, excellent thermal conductivity, and commercial availability. Corrosion behaviors of Fe- and Ni-base alloys have been extensively studied under simulated fuel cell interconnect exposure conditions [11]. Metal loss and scale morphology results show that Fe-based austenitic or ferritic alloys experience accelerated localized corrosion in the oxidant gas under a dual atmosphere or bi-polar (simultaneous exposure to fuel and oxidant gases) conditions compared to exposure to air-only environment and hence are less preferred.

2.3.4 Electrolyte

The electrolyte for solid oxide fuel cell must be stable in both reducing and oxidizing environments and must have sufficiently high ionic with low electronic conductivity at cell operating temperature. In addition the material must be able to be formed into a thin strong film with no gas leaks. The required properties for these materials, fixed by both electrochemical constraints and high operating temperature, are the following [8]:

1. High ionic conductivity ($\geq 0.1 Scm^{-1}$ at 900^0C)
2. Phase stability from room temperature to 1100°C approximately.
3. Thermal expansion coefficient compatible with other cell components.
4. Chemical compatibility with electrode and interconnection materials and with oxygen and fuel gas as well.
5. Gas tightness
6. Fracture toughness (>400MPa at room temperature)
7. Moderate cost of materials and fabrication.

Various electrolytes have been studied. Each one has some advantage and disadvantage. In the following section, their properties have been summarized;

2.3.4.1 Yttria Stabilized Zirconia

The material used as the solid electrolyte in most of the fuel cells is Yttria-stabilized zirconia (YSZ), because of its higher conductivity and desirable stability in both oxidizing and reducing

atmospheres [8, 9]. High-temperature zirconia (ZrO_2) has the cubic fluorite structure. On cooling from its melting point (2680°C), it transforms to a tetragonal form at 2370°C and then to a monoclinic form at 1170°C. The high-temperature structure can be stabilized to room temperature by substitution of larger cations of lower valence (e.g.,$Zr_{1-x}Ca_xO_{2-x}$ or $Zr_{1-x}Y_xO_{2-0.5x}$) for Zr^{4+}, which also introduces oxygen vacancies on the normal sites and therefore oxide-ion conductivity. The amount of dopant required to fully stabilize the cubic structure is about 12–13 mol% for CaO, 8–9 mol% for Y_2O_3 and Sc_2O_3, and 8–12 mol% for other rare-earth oxides. The tetragonal phase is stabilized with low-dopant content, i.e., about 2 to 2.5 mol% for Y_2O_3 and several other rare-earth oxides. The cubic phase has low strength, toughness, and thermal shock resistance, whereas the tetragonal phase has extremely high strength and toughness due to a stress-induced phase transformation to monoclinic zirconia. Stabilized zirconia, however, requires an operating temperature of ~ 1000°C due to desirable conductivity requirements. Various problems are associated with such a high temperature: thermal stresses at the electrolyte-electrode and electrode-interconnect interfaces, inter diffusion between electrodes and electrolyte. A substantial effort has been made to develop electrolytes, alternative to stabilized zirconia, with higher ionic conductivity at lower temperatures.

2.3.4.2 Ceria Doped Alkaline earth oxides

Some types of solid electrolytes have relatively high ionic conductivity at intermediate temperatures. Ce based oxide ionic conductors, such as Gd doped CeO_2, have a significantly higher ionic conductivity than most zirconia-based electrolytes and are a suitable basis material for intermediate temperature (500-600 °C) operation of SOFCs but they need a protective coating of a stable electrolyte on the fuel side because under anode environment they may become ionic/electronic mixed conductors [9]. The resulting “composite solid electrolyte” exhibit high ionic transport number, an output voltage close to the theoretical value, and higher conductivity than a single phase YSZ in the temperature range 600-800°C. Development of other materials, especially those possessing sufficiently high ionic conductivities at intermediate temperatures (600 - 800°C), has received much interest recently. In this connection several doped perovskite (ABO_3) solid electrolytes have been identified.

2.3.4.3 Bismuth oxide based electrolytes

Another promising material is bismuth based oxides [12, 13]. Stabilized bismuth oxide (Bi_2O_3) exhibits the highest ionic conductivity at comparable temperatures. This greater ionic conductivity of stabilized Bi offers the possibility of its use as an electrolyte in SOFCs operation at lower temperatures (<1000°C). Pure bismuth oxide has two thermo-dynamically stable crystallographic polymorphs. One is α-Bi_2O_3, which is stable below 730°C and has a monoclinic structure, which allows p-type conduction. The other is δ-Bi_2O_3, which is stable above 730°C, up to its melting temperature of 825°C, and crystallizes in the fluorite structure (cubic CaF_2) structure. In addition to these phases, tetragonal (β-Bi_2O_3) and body centered cubic (γ-Bi_2O_3) crystallographic modifications are also known to exist below 650°C, as meta stable phases. The high polarizability of the Bi^{3+} ion with its lone pair of electrons has been viewed as its conductivity enhancing factor. Another possibility could be the existence of a weaker metal oxygen bond between bismuth and oxygen as compared to that between zirconium and oxygen this might promote a greater mobility of the vacancies in the lattice. However the high conductivity phase is stable over a very narrow range of temperature (730-800°C). A large number of studies have shown that the high conductivity δ-phase in Bi_2O_3 could be stabilized at lower temperatures, by the addition of dopants. In some cases, doping leads to transformation into a more conducting rhombohedral phase which, however, undergoes decomposition which lead to decrease in ionic conductivity below 700°C temperature. Further the volume change associated with the δ→α phase transition leads to cracking and severe deterioration of the material. Thus for application of Bi_2O_3 as a solid electrolyte in fuel cells, it is imperative that the high temperature cubic phase is stabilized. The temperature dependence of conductivity of various solid electrolytes shows that Bi_2O_3 based material stand out as superior oxide electrolytes. However, the main drawback of this material is its small potential range of its ionic conduction. Bi_2O_3 is also prone to reduction into metallic bismuth, even at moderately low oxygen partial pressure [12].

2.3.4.4 Bi_2O_3 - M_2O_5 (M= V, Cu, Ti) system

A number of phase equilibria and ionic conductivity investigations have been carried out in the Bi_2O_3- M_2O_5 systems [14, 15]. The compound Bi_2O_3- V_2O_5 has a layered structure and undergoes several structural transitions between 405°C and congruent melting point, 887°C. Bismuth vanadate $Bi_4V_2O_{11}$ is the parent compound of an extensive range of substitutional solid solutions which have become known as the BIMEVOX family. $Bi_4V_2O_{11}$ shows complex polymorphism but essentially has three main polymorphs α→β (447°C) and β→ γ (567°C). Conductivities in the order of 10^{-1} Scm^{-1} have been reported at 600°C for the parent compound and a number of the substituted BIMEVOX. This behavior is believed to be combined result of a high concentration of anion vacancies and a disordering of the anion vacancies within the structure. At low temperatures the $Bi_4V_2O_{11}$ structures (α and β phases) becomes more ordered, the unit cells larger, and the conductivity markedly lower. The low temperature conductivity can be enhanced by stabilizing the disordered γ phase at room temperature, which can be achieved by the partial substitution of various metallic ions for vanadium and bismuth sites.

Cation substituted bismuth vanadate possesses high oxygen ion conductivity at lower temperatures. The ionic conductivity of this material at 300^oC is 50 to 100 times more than any other solid electrolyte. Three phases (α,β,γ) are observed in the substituted compound; α and γ are low and high conducting phase respectively. Substitution of vanadium in Bi4V201 I by various cations such as Li_{3+}, Zn_{2+}, $A1_{3+}$, Ti_{4+} and Ge_{4+} has been investigated [14,15] up to 10% of these cations substitute in Bi4V2011 stabilizing in α/γ phases. The γ phases are good oxygen-ion conductors just as the Cu_2+-substituted analogue. The 10% Ti_4+-substituted phase, Bi4V1.8Ti0.2010.9, is the best oxygen-ion conductor among the substituted bismuth vanadates investigated. It appears that the ionic potential of the substituting cation, rather than the oxygen vacancy concentration, is an important factor in determining the oxygen-ion conductivity of these materials. The various properties of above described electrolytes are given in table 2:

Table 2.1:- Comparison of various electrolyte materials [15]:

Properties / electrolyte	Operating temp (^oC)	Ionic conductivity, □ (S/cm)	Other features
ZnO-doped YSZ	800	0.0289	Degradation of the cell components and interfacial reaction
$GdAlO_3$, Ca-doped $GdAlO_3$	1000	0.0132, 0.057	New material with little data on its oxygen ion conductivity
ZrO_2 co-doped with Sc_2O_3 and CeO_2	800	0.120	High sintering temperature
BIMEVOX	400	0.02	Good stability over time, high density

2.3.5 Sealants

Development of reliable methods for sealing solid oxide fuel cell stacks presents the most challenging set of performance criteria in the entire field of ceramic joining. For SOFC applications, the functional requirements [16] and materials selection parameters of the SOFC seal are summarized in table 2.3:

Table 2.2: Required parameters of sealants for SOFC:

Mechanical	**Chemical**
• Hermetic/marginal leak rate	• Long –term chemical stability under simultaneous oxidizing/wet fuel environments
• TEC matching	
• Acceptable bond strength or compressive loading requirement	• Long-term chemical compatibility with the adjacent sealing surfaces
• Resistant to degradation due to thermal cycling/thermal shock	• Resistance to hydrogen embrittlement

Design/fabrication	**Electrical**
• Low cost	
• Facile processing and high reliability with respect to forming a hermetic seal	• Non-conductive (non-shorting configuration)
• Design flexibility	

2.3.5.1 Role of sealing material in SOFC

- To prevent mixing of fuel and oxidant within stack.
- To prevent leakage of fuel and oxidant outside the stack.
- Isolate electrically cells in stack.
- Provide mechanical bonding of the components.

2.3.5.2: Glass sealants:

A number of materials have been considered for compressive sealing, including, mica, nickel and copper, but each has been found deficient for several reasons, including the oxidation resistance in the case of metals to poor hermiticity and also the seal leakage in the case of mica [17, 18]

Material oxidation and load relaxation due to creep, as well as added expense and additional thermal mass that must be heated, cooled and maintained at temperature under the equilibrium operation are all issues that require particular attention with this type of cell design. Due to these constraints and specifically because our application is an auxiliary power unit (APU) where minimization of device weight and volume are critical, rigid seals are good choice such as glass sealants . The majority of SOFC seal development has focused on bonded, rigid seals; primarily glass and glass ceramics, which essentially "glue" the stack components together. Many glass seals are deigned to soften, and viscously flow above the SOFC operating temperature to provide hermetic seals by mechanical/chemical bonding. On cooling back down to operating temperature, the glass crystallizes to form a rigid, bonded seal. A principal advantage of glass seals is that the glass composition can be tailored to optimize some of the physical properties, such as thermal expansion coefficient (TEC).

2.3.5.3 Properties required for glass sealant

A sealing material has to fulfill some critical requirements as described above, because the operation temperature of the SOFC is almost 850°C and the operation period must be more than 5 years. Other major requirements are:

-No chemical reaction with the joining components and solder stability in oxidizing and wet reducing atmospheres;

Viscosity: 10^5 Pa-s at joining temperature (1000°C) and $>10^9$ Pa-s at operating temperature (850°C);

Only a small thermal expansion mismatch with respect to SOFC components (TEC=$11X10^{-6}$ K^{-1});

Leakage rate of joining should be less than 10-7 mbar 1s-1 per cm joined length;

However, several challenges remain with respect to the use of glass seals in SOFCs. The brittle nature of glasses below the glass transition temperature makes the seals vulnerable to crack formation, and glasses tend to react with other cell components, such as electrodes, at SOFC operating temperatures. Glass seals can affect electrode performance over a short range (via solid

state diffusion or viscous flow) or over longer distances (via gaseous transport of glass constituents).

Glass ceramics sealants are potential sealants because they can be tailored to optimize the physical properties and have greater resistance against corrosion as compared to other materials and are compatible with other components of SOFC.

2.3.5.4 Various glass- ceramics sealants systems

1. P_2O_5 Glasses-The main problem with these types of glasses is the volatisation of the phosphate phase leading to surface nucleated crystallization. Meta or pyro phosphate phases are formed which show poor stability at higher temperature in wet gas atmosphere. Thermal coefficient of expansion of phosphate does not match with YSZ.

2. B_2O_3 Glasses- These have low softening temperature and are volatile in nature. Alkali borosilicate is not suitable for large sealing area because of the thermal mismatching and also at higher temperature glass forming agent B_2O_3 is lost.

3. SiO_2 Glasses- these are the best available glass sealant. Alkali silicate glasses are not used because they interact with other components of fuel cell. Alkaline earth aluminosilicate glass sealants are generally used because of following properties:

- High resitivity
- High thermal expansion (matching TEC with other components)
- Glass ceramics

Table 2.3: different glass sealing materials are summarized in tabular form as shown below:

Various glass systems	Different features of glass systems
P_2O_5 Glasses	Low TEC, low strength, reaction at anode, water soluble
B_2O_3 Glasses	Volatile, low softening temperature
SiO_2 Glasses	Best available glass sealants Alkaline earth aluminosilicate glass sealant

The most common sealants for SOFCs are glass or glass–ceramic materials, and have been shown to operate in fuel cells for more that 1000 h with no significant degradation. Many glasses and glass–ceramics generally used for sealants contain alkali metals. Although some alkali metal containing glasses have been used for sealants in SOFCs, they are generally avoided because they react with other fuel cell components and can enhance the volatility of chromium, which can lead to poisoning of the cathode. For SOFC applications, alkaline-earth-based glasses are more commonly used.

Two important criteria for selection of a suitable glass sealant are the glass transition temperature (*T*g) and the coefficient of thermal expansion (TEC). The glass transition temperature is important because the glass must flow sufficiently to provide an adequate seal, while maintaining sufficient rigidity for mechanical integrity. The coefficient of thermal expansion must match other cell components, such as the yttria-stabilized zirconia (YSZ) electrolyte and the interconnect material, to minimize thermal stresses. Most of the promising compositions are barium-containing glass–ceramics, which have relatively large coefficients of thermal expansion. Glass–ceramics are formed by the deliberate and controlled crystallization of a glass, which typically increases the strength and allows for control of the properties through control of the

amount and nature of the crystalline phase. In the case of barium-containing glass–ceramics for SOFCs, the crystallization increases thermal expansion. For example, coefficients of thermal expansion of $BaO–MgO–SiO_2$ and $BaO–ZnO–SiO_2$ increase with increasing BaO content for constant SiO_2 contents. This increase in coefficient of thermal expansion is due to the formation of barium silicate ($BaSiO_3$), which has a large coefficient of thermal expansion, as compared to, for example, enstatite ($MgSiO_3$). Barium aluminosilicate glass–ceramics crystallize to form celsian ($BaAl_2Si_2O_8$) in addition to, or instead of, barium silicate.

Other alkaline-earth oxides do not dissolve in the celsian phase, but rather form other phases. Calcium oxide is often added to form barium–calcium aluminosilicate (BCAS) sealants, in which case an additional phase, barium calcium orthosilicate phase ($Ba_3CaSi_2O_8$), with a desirably large coefficient of thermal expansion, is formed during crystallization [17]. The addition of magnesium oxide to barium aluminosilicate glass–ceramics results in the formation of enstatite ($MgSiO_3$) and silica along with celsian. There is a strong tendency for celsian formation as evidenced by the formation of celsian with only 3% BaO and the presence of only celsian and barium silicate in a glass containing 15%MgO. Magnesium aluminosilicates without barium oxide form cordierite ($Mg_2Al_4Si_5O_{18}$), which has a very low coefficient of thermal expansion.

The crystallization of barium aluminosilicate glasses is faster than that of the corresponding calcium and magnesium aluminosilicate glasses. The lower activation energy for crystallization with barium as the network modifier has been attributed to the lower field strength of barium as compared to calcium and magnesium. Thus, barium aluminosilicate glasses crystallize more fully and at lower temperatures as compared to those based on other alkaline-earth cations.

When using a glass–ceramic as a sealant, the glass should wet the surfaces to be bonded or sinter to full density before crystallization, which decreases the viscosity of the glass, so the optimal crystallization rate depends on the flow characteristics of the glass. If crystallization occurs before complete wetting or sintering occurs, poor adherence or porosity can result. Conversely, insufficient crystallization may lead to inadequate mechanical properties.

Boron oxide is an important addition to silicate glasses. Boron oxide is most commonly added to decrease the viscosity of the glass, and has been shown to decrease the softening point and glass

transition temperature of SOFC sealants. Boron oxide also increases the coefficient of thermal expansion, for compositions in which only the B_2O_3/SiO_2 ratio is changed. However, the effect of boron oxide on the coefficient of thermal expansion is overcome by other alloying additions for more complicated compositions. Boron oxide consistently leads to a decrease in the glass transition temperature.

Another important component of glass–ceramics is aluminum, which can have tetrahedral coordination and replace silicon in the glass network, but at larger concentrations acts as a network modifier. This dual role of aluminum has led to reports of aluminum both inhibiting and enhancing crystallization. Aluminum additions have also been reported to inhibit cristobalite formation, which as previously mentioned can cause cracking.

Although silicates are the most common ceramic glass sealants, other systems have been investigated. For example, phosphate-based systems have been developed. These glasses, however, typically have low coefficients of thermal expansion.

Some silica based glass sealants are studied and result obtained for sealant $SrO\text{-}La_2O_3\text{-}Al_2O_3\text{-}B_2O_3\text{-}SiO_2$ was that with high B_2O_3, very low softening points. For $BaO\text{-}Al_2O_3\text{-}B_2O_3\text{-}SiO_2\text{-}As_2O_3$ glass sealant, volatilization of B_2O_3 and As_2O_3 (pore formation) occurred. Crystallization rate were adjustable with MgO additions; interactions with interconnect alloy ($MgCr_2O_4$) occurred. For $AO\text{-}Al_2O_3\text{-}B_2O_3\text{-}SiO_2$ (A = Ba, Ca, Mg), sealant containing Ba had Higher CTE, lower Tg than Ca, Mg. For sealant $CaO\text{-}Al_2O_3\text{-}SiO_2$, Primary crystallization product: Wollastonite ($CaSiO_3$) was formed.

Table 2.4:- Coefficients of thermal expansion of crystalline phases formed in alkaline-earth glass–ceramics [17]

Systems	Major crystalline Phases	TEC ($°C^{-1} \times 10^6$)
Mg–Si–O	Enstatite (MgSiO3)	7–9
Ca–Si–O	Wollastonite (CaSiO3)	4–9
	Calcium orthosilicate (Ca2SiO4)	10–14
Ba–Si–O	Barium silicate (BaSiO3)	9–13
	Barium orthosilicate (BaSi2O5)	14
Ba–Ca–Si–O	Barium calcium orthosilicate (Ba3CaSi2O8)	12–14
Mg–Al–Si–O	Cordierite (Mg2Al4Si5O18)	1
Sr–Al–Si–O	Hexacelsian (SrAl2Si2O8)	8–11
	Monocelsian (SrAl2Si2O8)	3
	Orthocelsian (SrAl2Si2O8)	5–8
Ba–Al–Si–O	Hexacelsian (BaAl2Si2O8)	7–8
	Monocelsian (BaAl2Si2O8)	2–3
	Orthocelsian (BaAl2Si2O8)	5–7

CHAPTER 3

LITERATURE REVIEW

In this chapter, interaction of various glass sealants with electrolytes and high ionic conductivity electrolytes at low temperature has been summarized. The chemical compatibility of glass–ceramic sealants with the yttria-stabilized zirconia electrolyte is extensively studied. Silicates containing barium, calcium and/or magnesium have been reported to form adherent and stable interfaces with yttria-stabilized zirconia.

D. Bahadur et al. [19] studied the chemical interactions between different MgO-SiO2-Al2O3-B2O3 base glass sealants and components of solid oxide fuel cells. The SOFC materials considered are ZrO2 stabilized with 8 mol % Y2O3 (as electrolyte and part of the Anode), Ni (as part of the anode), and the oxide-dispersion-strengthened (ODS) alloy Cr5Fe1Y2O3 (as interconnect). Glass compositions with no nucleating agent and with ZrO2, Cr2O3, or Ni as the nucleating agents were prepared. Powder mixtures of these sealants with the mentioned SOFC materials, as well as the sealant/material interfaces, were characterized by X-ray diffraction and scanning electron microscopy and energy dispersive spectroscopy in order to determine possible reaction phases and the diffusion behavior of different cations. The powder mixtures of various glass sealants with YSZ annealed at 1000°C for 100 h were studied. Additional phase $ZrSiO_4$ was detected in all samples as the dominant product phase. Moreover, the product phases Mg2SiO4 and MgSiO3 were present in the powder mixtures. Formation of cordierite and cristobalite as detrimental phases was detected in many of the mixtures. The formation of these phases can be suppressed if Cr2O3 or Ni is added to the glass as the nucleating agent. The most interesting feature of these results is the absence of the cordierite phase for all reaction powder mixtures if Cr2O3 is used as the nucleating agent.

Yang et al. [20] studied the compatibility of the Barium-Calcium-Alumino silicate glass sealants with the interconnect AL29-4C (Cr 29%, C 0.01, Mg 0.2%, Fe balance) and the electrolyte YSZ. Through heat treatment in air(850° C for 1 h followed by 750° C for 4 h), a coupon of interconnector was joined to an ideally sized YSZ plate by the sealant to form a joined couple. The joined couple was analyzed by SEM and a scan of the cross sectional revealed an inhomogeneous microstructure along interconnect/sealant interface and a homogeneous one along sealant/electrolyte interface. Some penetration of the glass-ceramics into YSZ was evident, which likely resulted in strong bonding between the glass sealant and YSZ plate via mechanical interlocking.

Jinnapat et al. [21] studied the ceramics seal for solid oxide fuel cell. In the study, several ceramics adhesives and glass composites have been investigated for use as a sealing material for SOFC based on yttria-stabilised-zirconia oxide(YSZ) electrolyte and stainless steel interconnector system in operating conditions of SOFC at 800° C. borosilicate glass was used as sealant and softening temperature is close to operating temperature so sealing properties were really good. Boron oxide vapor is produces both in oxidizing and reducing environment and the glass react with YSZ pallets after 200 h at 800- 1000 ° C.

Sohn et al. [22] investigated bonding characteristics and wetting behavior of the $BaO–Al_2O_3$-$B_2O_3–SiO_2$ system with the addition of La_2O_3, ZrO_2, or NiO glasses to YSZ by observing shape change of the glass pellet on the YSZ plate with increased temperature. The powdered glass pellet, placed on the YSZ plate, was heated to 950°C at a rate of 5°C/min and held for 30 min to bond the glass and YSZ together. The resulting glass/YSZ specimen was cooled slowly to 900°C at a rate of 3°C/min and held at that temperature for 3 h to allow crystallization of the glass on the YSZ and then cooled to room temperature at a rate of 5°C/min. Consequently, some of these glass-ceramics were confirmed to have formed a long-term, chemically stable interface with the YSZ in an air atmosphere. However, the glass-ceramics from 2% ZrO_2 at constant ratio of SiO_2/B_2O_3 =0.5 and with 5% ZrO_2 at the constant ratio of SiO_2/B_2O_3= 0.70 parent glasses showed a significant change in microstructure after long term heat treatment at the operation temperature, whereas the glass-ceramic having La_2O_3 showed no micro structural change, even after heat treatment for up to 1000 h.

Goel et al. [23] studied the processing and the characterization of calcium-magnesium alumino silicate glass sealants and their compatibility with other components. The experimental results of wetting experiments suggest a strong interfacial adhesion between the four investigated compositions and 8YSZ at 900°C (100 h, air). In particular, a good wetting regime was observed (i.e., contact angle<90°) and continuous interfaces, with no cracks or gaps, were revealed after cross section and polishing. There was no evidence of a reaction at the interface, except in the case of glass sealant containing 13.02% BaO, where a thin reaction layer was observed, probably due to a B-rich liquid phase formed during heat treatment, favoring diffusion of components.

Lahl et al. [24] studied the chemical interactions between several aluminosilicate glasses and components at the anode side of SOFC. Severe reactions occur if the modifier ions are Ba and Ca. MgO base sealants have been investigated in detail. The formations of some detrimental phases were seen for the sealants containing MgO. Cordierite forms with many reaction mixtures of sealants with ZrO_2 stabilized with 8 mol % Y_2O_3 (as electrolyte) or nickel (as anode) when MgO based glass sealants were used. The phase m-ZrO_2 is formed during the interaction of glass containing CaO with 8YSZ, this is due to the diffusion of yttrium from 8YSZ into the glass. However, the cordierite phase is not formed by this interaction if the glass containing MgO with 2% of TiO_2 is used as a nucleating agent.

Chen et al. [25] studied interface reactions between the metallic plates interconnect and electrolyte (YSZ) with the sealant BaO-B_2O_3-SiO_2-Al_2O_3. The results show that the crystalline phases of 45BaO- 20B_2O_3-35SiO_2-10Al_2O_3 glass are Celsian and its polymorph, Hexacelsian, and Barium Silicate. Glass bulk placed on YSZ and Crofer 22 plates were heated up to 900°C at 10°C/min and held for 10 min in order to bond the glass and YSZ/Crofer 22 plates together, then the resulting specimens were cooled down to 650°C, maintained for 10 and 50 hr. From the EDS result, no elements in glass diffused toward YSZ were found, but the diffusion of zirconium toward glass is found irrespective of heat-treatment temperature and time. Therefore, a zirconium rich needle-shaped crystal was found in glass. Because of the CTE mismatch, not only cracks were formed along and inside the crystalline phase, but also a gap was formed between the parent glass and the reaction layer.

Meinhardt.et.al [26] studied the interaction of glass sealant BaO-CaO-Al_2O_3-SiO_2-B_20_3 (BaO 35%, CaO 15%, Al_2O_3 5%, SiO_2 35%, B_2O_3 10%) with ytteria stabilized zirconia operated at 750° C for 1200 hours. It showed the minimum interaction as very small amounts of $BaZrO_3$ phase was at the surface of the YSZ and is almost compatible with the sealant as shown in figure below.

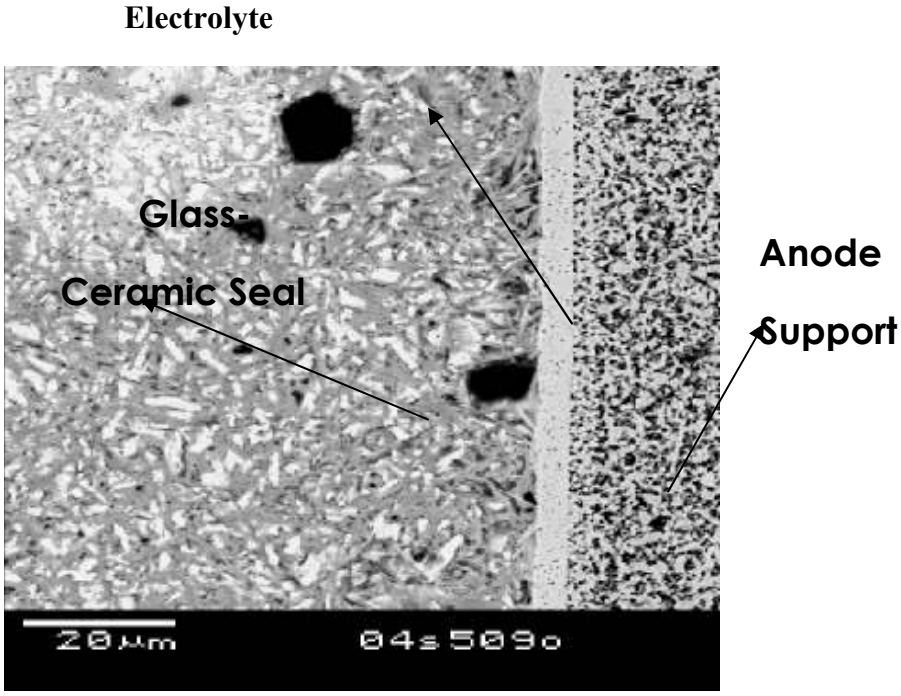

Fig 3.1: Microstructure showing interaction of glass sealant with YSZ electrolyte

Singh et al. [14, 15, 27] studied that cations substituted bismuth vanadate possesses high oxygen ion conductivity at lower temperatures. The ionic conductivity of this material at 300^{o}C is 50 to 100 times more than any other solid electrolyte. Three phases (α,β,γ) are observed in the

substituted compound; α and γ are low and high conducting phase respectively. Samples of $Bi_4V_{2-x}M_xO11_{-\delta}$ (x = 0 to 0.4) with (M= Ti^{+4}, Cu^{+2}, Al^{+3}) were prepared by solid state reactions technique. The high temperature, high oxide ion conducting γ-phase of $Bi_4V_2O_{11}$ is stabilized for $Bi_4V_{2-x}Cu_xO_{11-\delta}$ with $x \geq 0.2$.

A. Goel et al. [28] studied the effect of Cr_2O_3 addition on crystallization and properties of La_2O_3-containing diopside glass-ceramics. The experimental results of wetting experiments suggest strong interfacial adhesion between the four investigated compositions and 8YSZ at 900 °C (1 h, air) . In particular, a good wetting regime was observed (i.e., contact angle <90°) and continuous interfaces, with no reaction zones, cracks or gaps, were revealed after cross-section and polishing. No reaction products were also determined by XRD analysis of compact samples made of the powder mixtures of glasses and 8YSZ after heat treatment under similar conditions (i.e. 900 °C, 1 h).

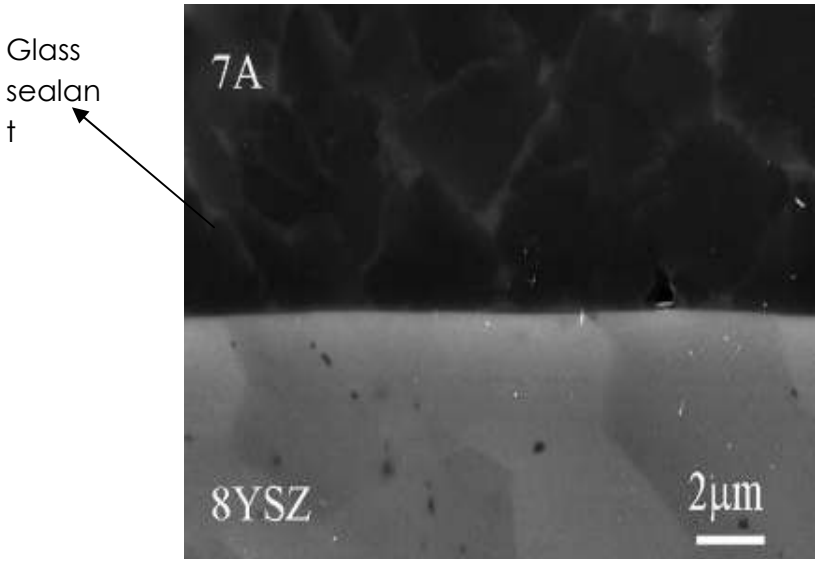

Fig 3.2: Microstructure showing interaction of glass sealant containing $Cr_2O_3$with

YSZ electrolyte

CHAPTER 4

EXPRIMENTAL TECHNIQUES

4.1 Sample Preparations

4.1.1 Glass sample preparation

Samples of the glass were prepared by mixing of the raw materials in the form of SiO_2, B_2O_3, Y_2O_3, Al_2O_3, La_2O_3, Cr_2O_3 and SrO using conventional melt-quenching techniques. The purity of constituent oxides which were used to prepare the samples was ≥ 99 %. Each batch was prepared by mixing an appropriate mole fraction of well desired initial ingredients using mortar and pestle. Sample compositions with their label are given in table 4.1:

Table 4.1: Glass compositions (mol %) with their label

Sample Label	**SiO_2**	**B_2O_3**	**SrO**	**Y_2O_3**	**La_2O_3**	**Al_2O_3**	**Cr_2O_3**
S1	40	20	30	10	0	0	0
S2	40	20	30	0	10	0	0
S3	40	20	30	0	0	10	0
S4	40	20	30	0	0	0	10

The mixed powders of these samples were placed in recrystallized alumina crucible and melted in an atomized Molybdenum Disilicide ($MoSi_2$) electric resistance furnace. The powders of the samples were initially kept at 1000ºC for 1 hour for calcination to occur and release of water from the starting materials then they were reheated at 1550ºC and kept at this temperature for half an hour in order to achieve the homogeneity. The melt was poured either in graphite mold or on the flat copper plate and quenched by other copper plate in air to obtain flakes.

4.1.2 Electrolyte preparation

$Bi_4V_{2-x}Al_xO_{11-\delta}$ (x= 0.2) powders was prepared by solid-state reaction from stoichiometric amounts of Bi_2O_3, V_2O_5, and Al_2O_3 oxides. The purity of all oxides was more than 99 %. The starting powders were mixed in acetone media in mortar pestle for an hour to break any large agglomerates then ball milled for 2 hours. This length of time was required to achieve a fully homogeneous powder mixture and to facilitate good reaction of the oxide powders. The resulting mixture was dried and thoroughly ground and then calcined at 700^oC in silica crucibles for 12 hrs. Calcined powder was ground, mixed and refired at 800^oC for 12 hrs. The sintered powder was further ground and compacted at a pressure of 10 ton after mixing with PVA binder to make pellets of approximately same dimensions. The approximate pellets dimensions were 20 mm diameter by 3 mm thickness. The so prepared pellets were sintered at optimum temperature of 800^oC for 10 hrs.

4.1.3 Sample preparation for interaction study

For the interaction study the glass samples (as given in table 4.1) and Bi- based electrolyte were grinded in 3:1 wt % ratio respectively in the mortar pestle. The mixtures of both the samples were grinded for 1 hr to obtain the fine homogeneous powder. The mixed powders of these samples were placed in recrystallized alumina crucible fir 1 hr heat treatment at 800° C. The heat treated samples were taken out from the crucibles for various investigations such as X-ray diffraction (XRD) and Fourier Transform Infra-Red spectroscopy (FTIR). The mixtures were

now heat treated at 800°C for 10 hrs and 100 hrs durations. The various heat treated samples (1, 10, 100 hrs) are characterized using X-ray diffraction (XRD) and Fourier Transform Infra-Red spectroscopy (FTIR). Sample levels, compositions with different heat treated durations are given in the table 4.2. Sample preparation, heat treatment durations are also summarized in flow chart form.

Table 4.2: Different combinations of the glasses and electrolyte with heat treatment durations.

Sample Name	Glasses	Electrolyte (x=0.2)	Heat treatment durations(hrs)
IS1	$SrO\text{-}SiO_2\text{-}B_2O_3\text{-}Y_20_3$	$Bi_4V_{2-x}Al_xO_{11}$	1, 10 , 100
IS2	$SrO\text{-}SiO_2\text{-}B_2O_3\text{-}La_20_3$	$Bi_4V_{2-x}Al_xO_{11}$	1, 10 , 100
IS3	$SrO\text{-}SiO_2\text{-}B_2O_3\text{-}Al_20_3$	$Bi_4V_{2-x}Al_xO_{11}$	1, 10 , 100
IS4	$SrO\text{-}SiO_2\text{-}B_2O_3\text{-}Cr_20_3$	$Bi_4V_{2-x}Al_xO_{11}$	1, 10 , 100

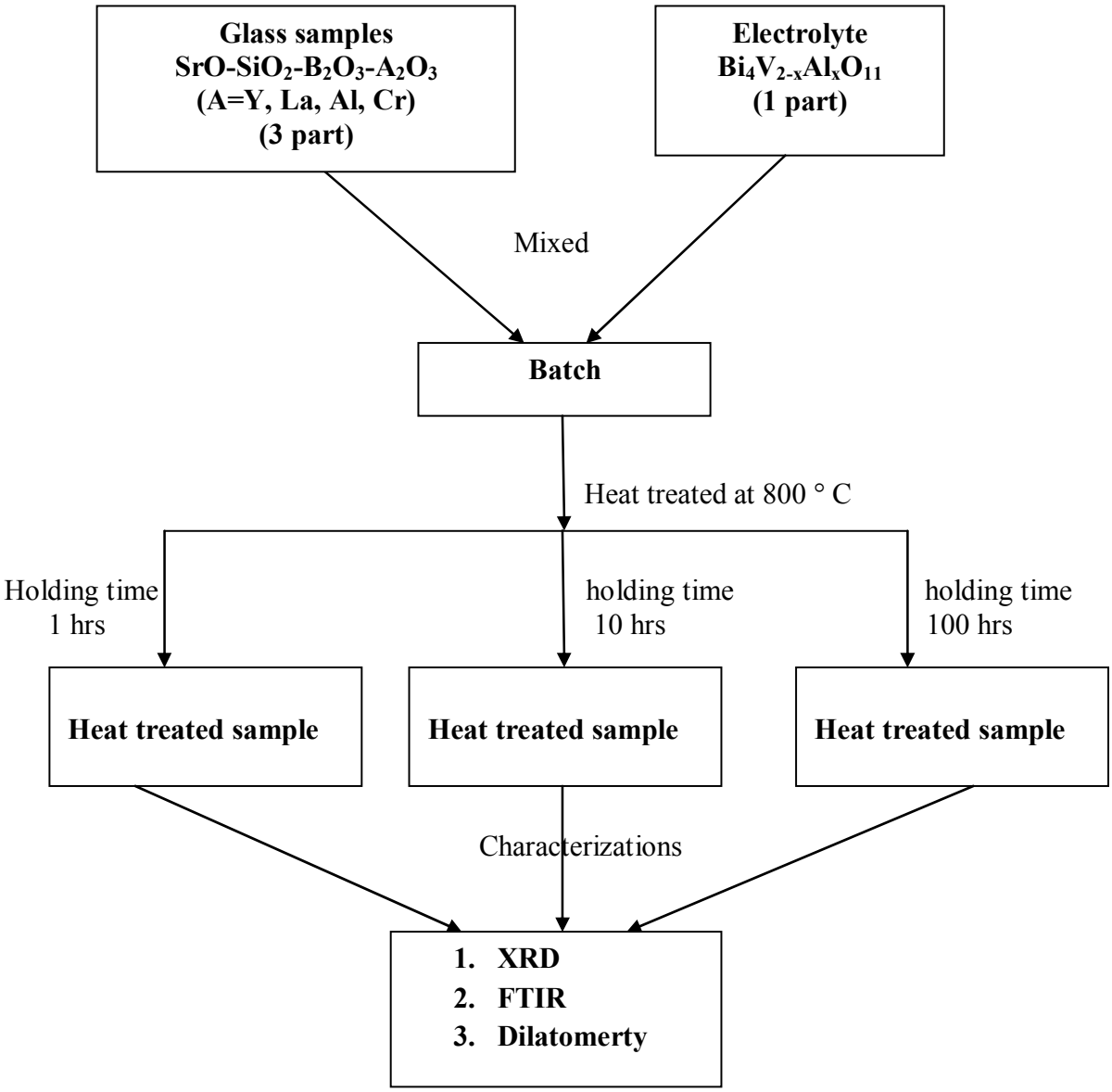

Fig 4.1: **Flow chart of sample preparation**

4.2 X-ray diffraction technique (XRD)

X-ray diffraction analysis (XRD) is a non-destructive, very versatile technique to determine the phase identification and volume fractions of crystalline materials. The sample is irradiated with monochromatic X-ray and the reflected radiation is recorded by the counters. In this technique various forms of the samples could be used and very less amount is required for phase determination. The X-ray diffraction patterns were recorded using Rigaku model Geiger diffractogram with $CuK_{\square}$ radiation (λ = 1.5418 Aº) obtained from copper target using an in built Ni filter. The 2□ values for XRD patterns were generally taken in the range of 5º to 80º for most of the samples at a scan speed of 5 degree per minute. Inter planar spacing (d) values of samples were calculated using the Bragg's law

$$2d \sin \square = n \lambda \qquad (1)$$

Where λ is the wavelength of incident X-ray, d is the interplanar distance and □ is diffraction angle. The XRD patterns were identified using standard Powder Diffraction files (PDF). Plotting the angular positions and intensities of the resultant diffracted peaks of radiation produces a pattern, which is characteristic of the sample. The experimental set up of X-ray diffraction is shown in fig 4.4

Fig 4.2: **Experimental set up of X-ray diffraction**

4.3 Fourier Transform Infrared Spectroscopy (FTIR)

Infrared spectroscopy is very important technique for materials analysis in the laboratory for over seventy years. An infrared spectrum represents a fingerprint of a sample with absorption peaks which correspond to the frequencies of vibrations between the bonds of the atoms making up the material. Because each material is a unique combination of atoms, no two compounds produce the exact same infrared spectrum. Therefore, infrared spectroscopy can result in a positive identification (qualitative analysis) of every different kind of material. In addition, the size of the peaks in the spectrum is a direct indication of the amount of material present. With modern software algorithms, infrared is an excellent tool for quantitative analysis simply, it is the absorption measurement of different IR frequencies by a sample positioned in the path of an IR beam. The main goal of IR spectroscopic analysis is to determine the chemical functional groups in the sample. Using various sampling accessories, IR spectrometers can accept a wide range of sample types such as gases, liquids, and solids. Thus, IR spectroscopy is an important and popular tool for structural elucidation and compound identification. For most common materials, the spectrum of an unknown can be identified by comparison to a library of known compounds.

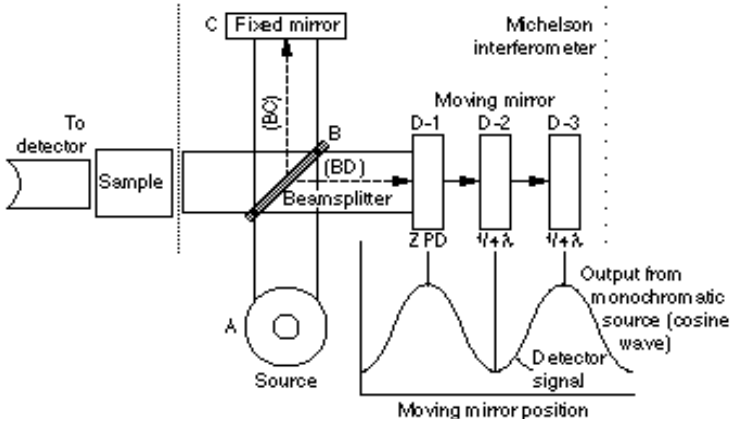

Fig 4.3 Simplified optical layout of a typical FTIR spectrometer

4.3.1 Spectrometer Components

There are three basic spectrometer components in an FT system: radiation source, interferometer, and detector. A simplified optical layout of a typical FTIR spectrometer is illustrated in Fig. 4.1. The same types of radiation sources are used for both dispersive and Fourier transforms spectrometers. However, the source is more often water-cooled in FTIR instruments to provide better power and stability. In contrast, a completely different approach is taken in an FTIR spectrometer to differentiate and measure the absorption at component frequencies. The monochromator is replaced by an interferometer, which divides radiant beams, generates an optical path difference between the beams, and then recombines them in order to produce repetitive interference signals measured as a function of optical path difference by a detector. As its name implies, the interferometer produces interference signals, which contain infrared spectral information generated after passing through a sample. The most commonly used interferometer is a Michelson interferometer. It consists of three active components: a moving mirror, a fixed mirror, and a beam splitter (Fig.4.1). The two mirrors are perpendicular to each other. The beam splitter is a semi reflecting device and is often made by depositing a thin film of germanium onto a flat KBr substrate. Radiation from the broadband IR source is collimated and directed into the interferometer, and impinges on the beam splitter. At the beam splitter, half the IR beam is transmitted to the fixed mirror and the remaining half is reflected to the moving mirror. After the divided beams are reflected from the two mirrors, they are recombined at the beam splitter. Due to changes in the relative position of the moving mirror to the fixed mirror, an interference pattern is generated. The resulting beam then passes through the sample and is eventually focused on the detector.

IR Frequency Range and Spectrum Presentation

Infrared radiation spans a section of the electromagnetic spectrum having wave numbers from roughly 13,000 to 10 cm^{-1}, or wavelengths from 0.78 to 1000 μm. It is bound by the red end of the visible region at high frequencies and the microwave region at low frequencies. IR

absorption positions are generally presented as either wave numbers or wavelengths (□). Wave number defines the number of waves per unit length. Thus, wave numbers are directly proportional to frequency, as well as the energy of the IR absorption. The wave number unit (cm^{-1}, reciprocal centimeter) is more commonly used in modern IR instruments that are linear in the cm^{-1} scale. In contrast, wavelengths are inversely proportional to frequencies and their associated energy. At present, the recommended unit of wavelength is μm (micrometers), but μ (micron) is used in some older literature.

IR absorption information is generally presented in the form of a spectrum with wavelength or wave number on the x-axis and absorption intensity or percent transmittance on the y-axis.

4.4 DILATOMETRY

A dilatometer measures the expansion of a material when it is heated. A small sample of the material is placed into the instrument and then heated (or cooled) according to a schedule picked by the investigator.

4.4.1 Working Principle of dilatometry

In a dilatometer the dimensional change is measured by subjecting a sample to a change in temperature. In principle, one can devise a simple arrangement in which the movement is transmitted out of the controlled environments and into the ambient by holding the sample between two rods which extend outside of the heated region as shown in figure 4.7. The sample pushes the two rods (A and B) as it is being heated, hence the name "pushrod". The sample will expand an amount shown by the shaded area, □L_S. By examining the experimental model, it becomes immediately clear that this configuration will not produce the desired □L_S. Since portions of both rods A and B are in the controlled environment, it is inevitable that they themselves will also expand (□L_A and □L_B respectively). Thus, the measured value of

($\Delta X_A+\Delta X_B$) will contain ($\Delta L_A+\Delta L_B$) in addition to ΔL_S. The sample's length change, ΔL_S, can therefore be written as:

$$\Delta L_S = (\Delta X_A - \Delta L_A) + (\Delta X_B - \Delta L_B) \ldots\ldots\ldots\ldots\ldots(2)$$

Unless one can assign values to ΔL_A and ΔL_B, the true magnitude of ΔL_S cannot be determined from the measured values of ΔX_A and ΔX_B alone. Obviously, if ΔL_A and ΔL_B are not present at all, the measurement becomes absolute, but as long as this is not the case, the measurement is, in principle, a relative one.

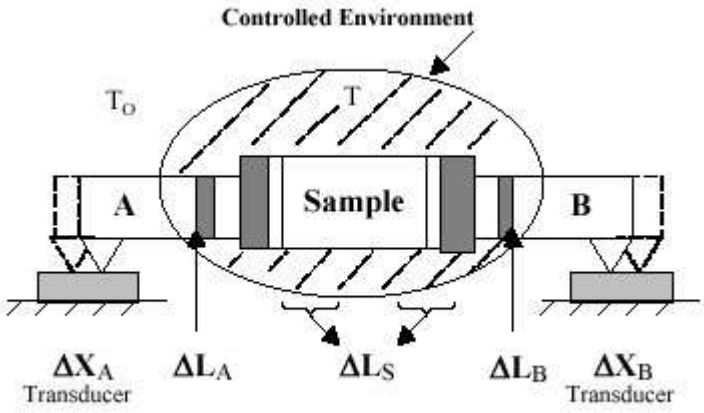

Fig. 4.4 Diagrammatic representation of sample holder (top view)

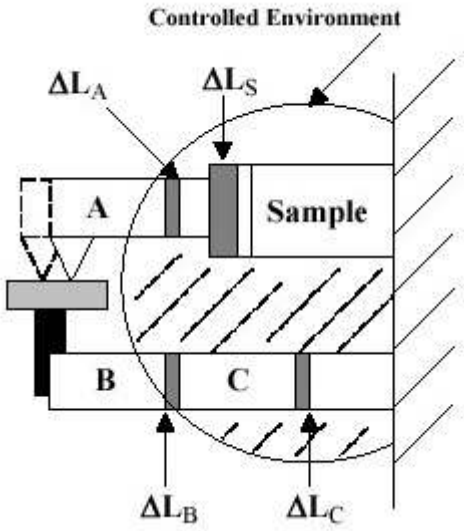

Fig. 4.5 Diagrammatic representation of sample holder (side view)

The most tempting prospect is to minimize the magnitudes of ΔL_A and ΔL_B in comparison to ΔL_S and then to neglect them. If the material of rods A and B do not expand appreciably compared to the sample, or not at all, the conditions become favourable to obtain results with reasonable accuracy. A good example of this would be to use light beams that do not expand when entering the controlled environment in place of rods A and B. More frequently, very low expansion materials such as fused silica are used for rods A and B, and, for many applications, this is enough to reduce inaccuracies to a small fraction of the measured values when high expansion materials such as plastics are tested.

In general usage, however, one must determine the magnitude of ΔL_A and ΔL_B accurately. Most commonly, one tests a sample from a material already well-defined by some other absolute method (twin telescopes, interferometer, etc.), which then leaves only the combined values of ΔL_A and ΔL_B unknown. This process is known as "calibration" for the dilatometer; the well-defined material is referred to as a "standard" or "reference;" and the combined value of ΔL_A and ΔL_B and is known as "system correction." Upon closer examination, it is clear that the correction obtained with a standard will be true only if this sample is of the same length, ensuring that the protruding lengths of rods A and B into the controlled environment region are identical during

the calibration and during the test. Furthermore, what may be true at one value of temperature T may not be true at another. To ensure that a calibration is indeed applicable: the sample and reference lengths must be close to each other. The calibration thermal cycle must closely approximate the test cycle (or vice versa). The reference's expansion must be close to the expected expansion of the sample. A major drawback of this configuration is its susceptibility to errors due to transducer gain mis- adjustment or malfunctions. Additionally, the high magnification severely restricts the range of measurable displacement. For these reasons, the use of differential dilatometers should be limited to applications in which the advantages clearly outweigh these drawbacks. If a temperature change from T_O to T has caused this expansion in a sample of initial length L_O, the average coefficient of linear thermal expansion can be calculated as

$$a = (\Delta L_S / \Delta L_O)/(T - T_O) \quad \text{.....(3)}$$

This coefficient, often referred to as TEC, is only true for the temperature range T_O to T. (Note that the word "linear" should never precede the word "coefficient", as it always implies uniaxial expansion rather than linearity of the coefficient.

CHAPTER 6

RESULTS AND DISCUSSION

5.1 X-ray diffraction analysis

The heat treated samples are investigated using x-ray diffraction pattern. XRD pattern of samples are given in figures from 5.1 to 5.4:

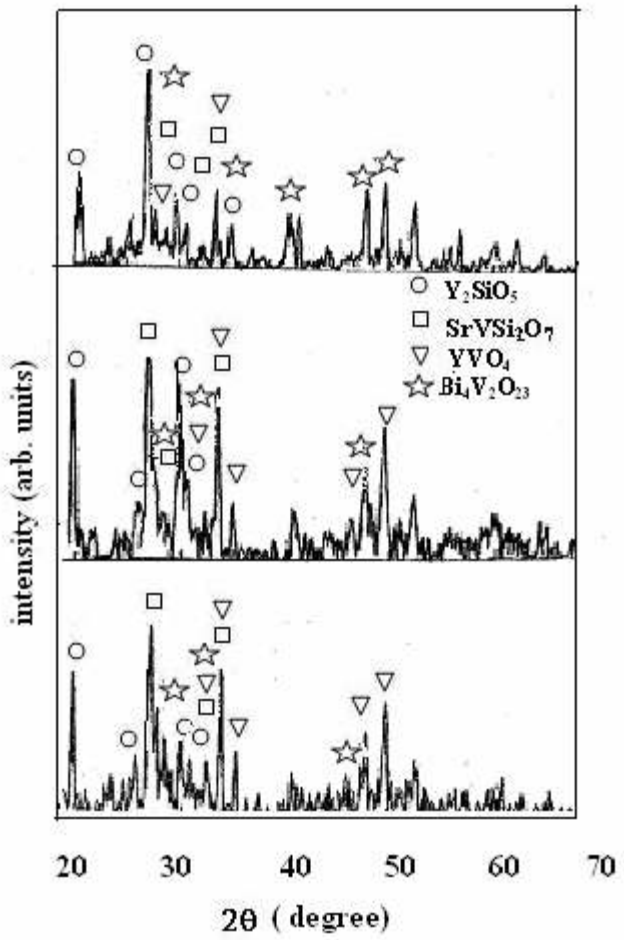

Fig. 5.1 XRD pattern for sample IS1 heat treated at (a) 1 hr, (b) 10 hrs and (c) 100 hrs

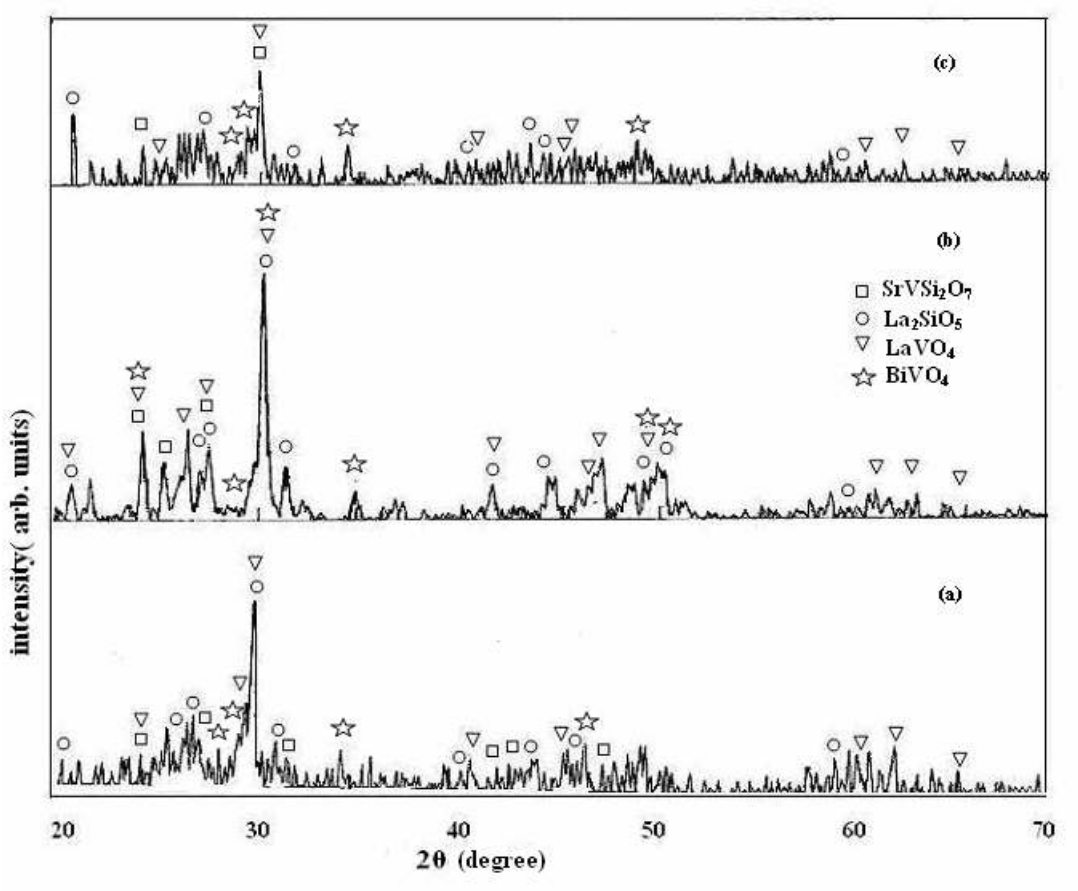

Fig. 5.2 XRD pattern for sample IS2 heat treated at (a) 1 hr, (b) 10hrs and (c) 100 hrs

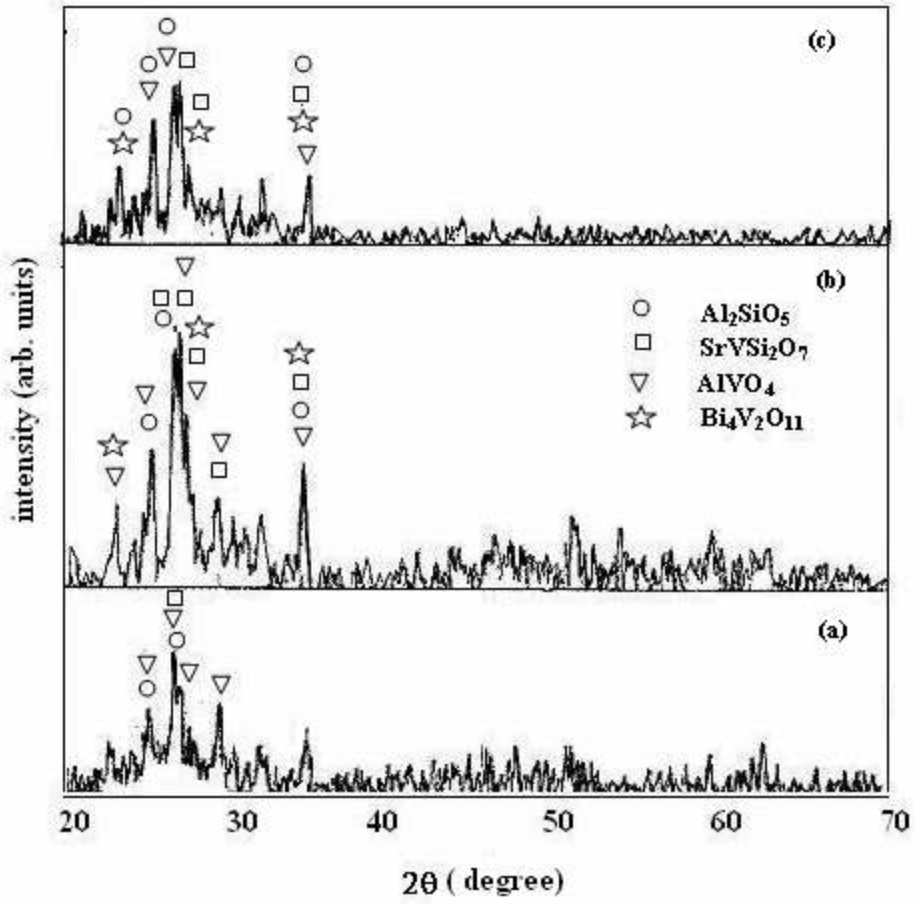

Fig. 5.3 XRD pattern for sample IS3 heat treated at (a) 1 hr, (b) 10hrs and (c) 100 hrs

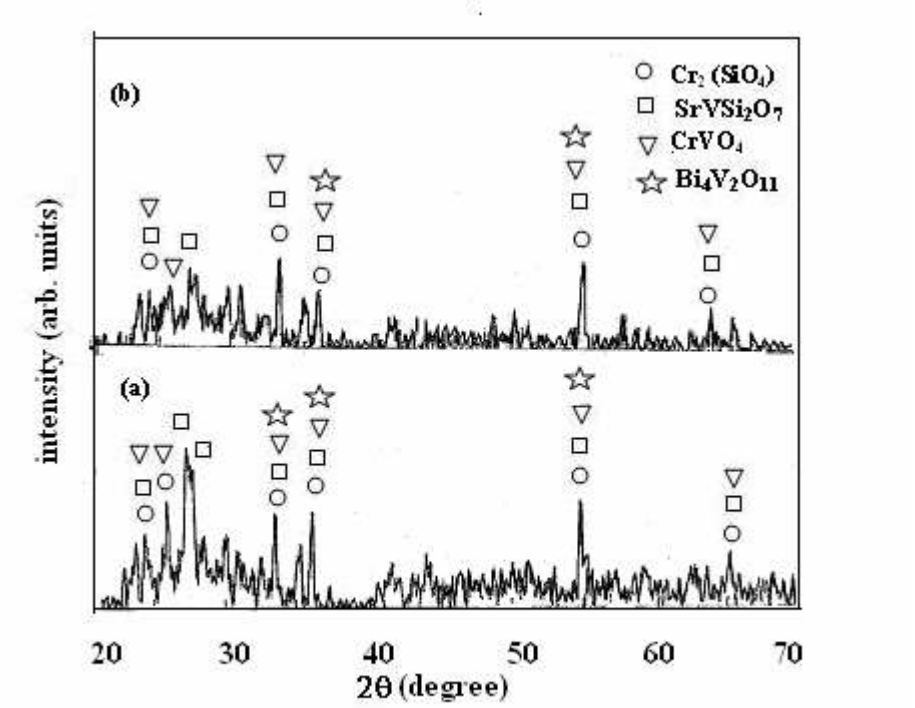

Fig. 5.4 XRD pattern for sample IS4 heat treated at (a) 10 hrs and (b) 100 hrs

Table 5.1: Crystalline phases and their volume fraction with different heat treatment durations for sample IS1:

Time duration(hrs)	Volume fraction the phases (%)			
	Y_2SiO_5	$SrVSi_2O_7$	YVO_4	$Bi_{12}V_2O_{23}$
1	24.01	32.57	25.33	18.1
10	27.56	31.73	26.28	14.42
100	44.6	17.86	20	17.86

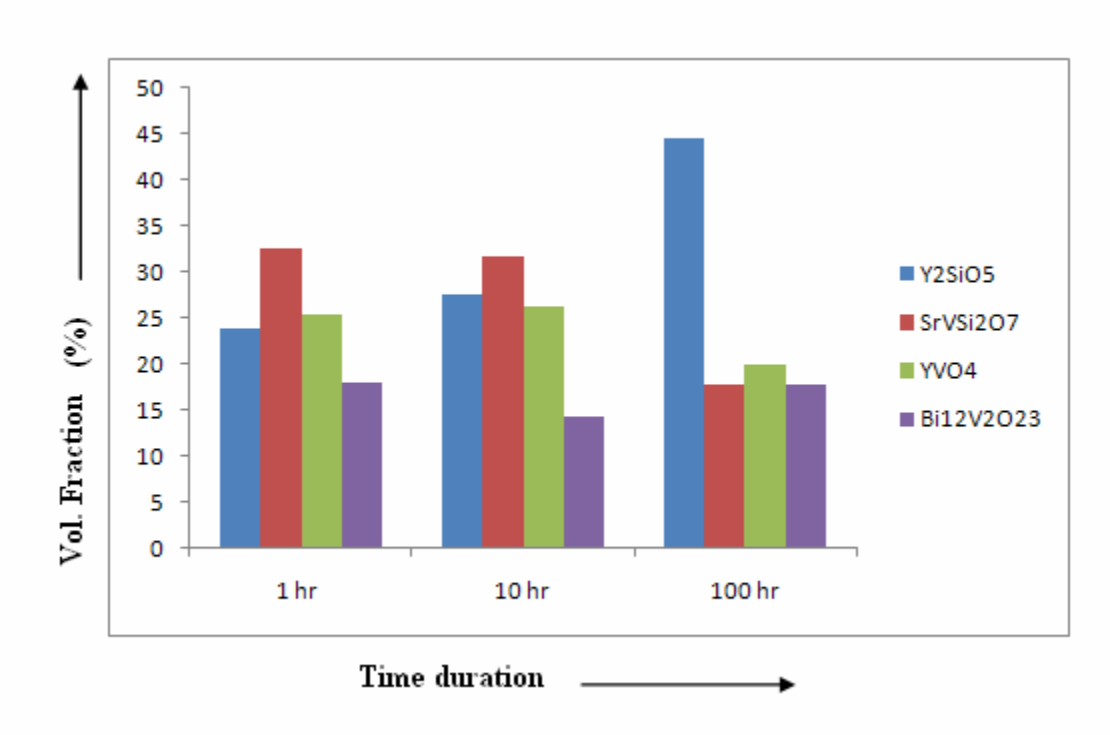

Fig 5.5: Variation of volume fraction of phases with increase in time duration of heat treatment for IS1 sample.

Table 5.2: Crystalline phases and their volume fraction with different heat treatment durations for sample IS2:

Time duration(hrs)	Volume fraction the phases (%)			
	La_2SiO_5	$SrVSi_2O_7$	$LaVO_4$	$BiVO_4$
1	39.47	9.65	39.47	11.4
10	27.7	16.7	27.7	27.7
100	23.26	32.56	32.56	11.62

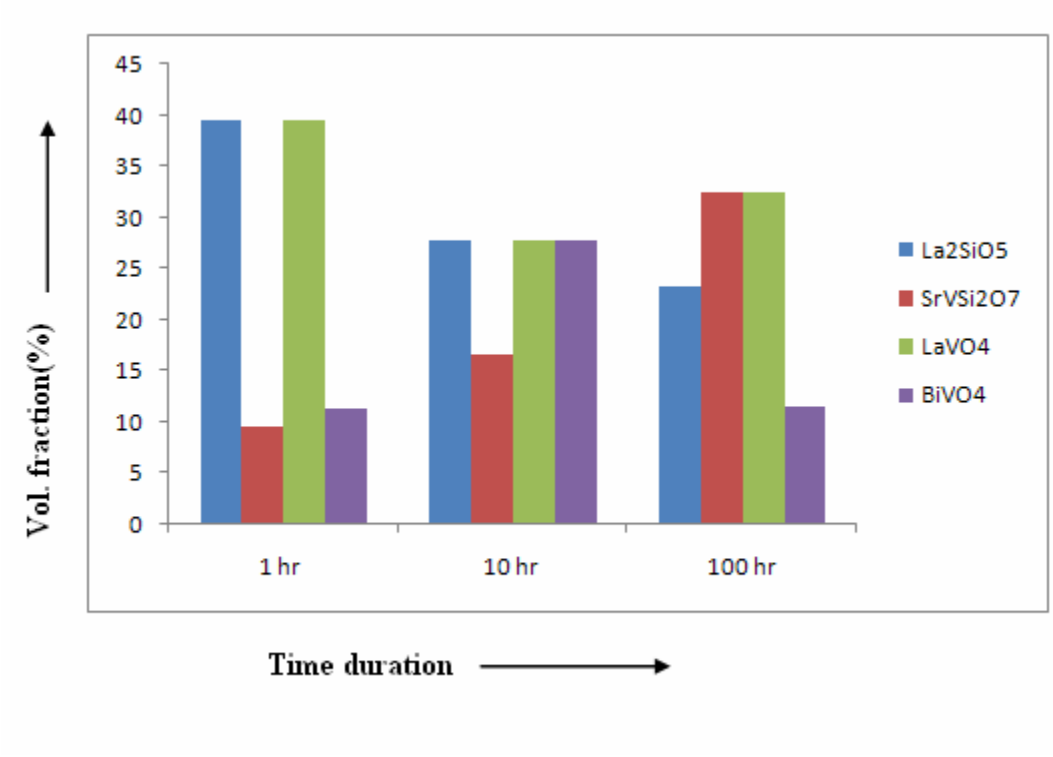

Fig 5.6: Variation of volume fraction of phases with increase in time duration of heat treatment for IS2 sample.

Table 5.3: Crystalline phases and their volume fraction with different heat treatment durations for sample IS3:

Time duration(hr)	Volume fraction the phases (%)			
	Al_2SiO_5	$SrVSi_2O_7$	$AlVO_4$	$Bi_4V_2O_{11}$
1	30.53	34.74	34.74	
10	24.64	28.69	28.69	17.97
100	23.6	30.74	30.12	15.52

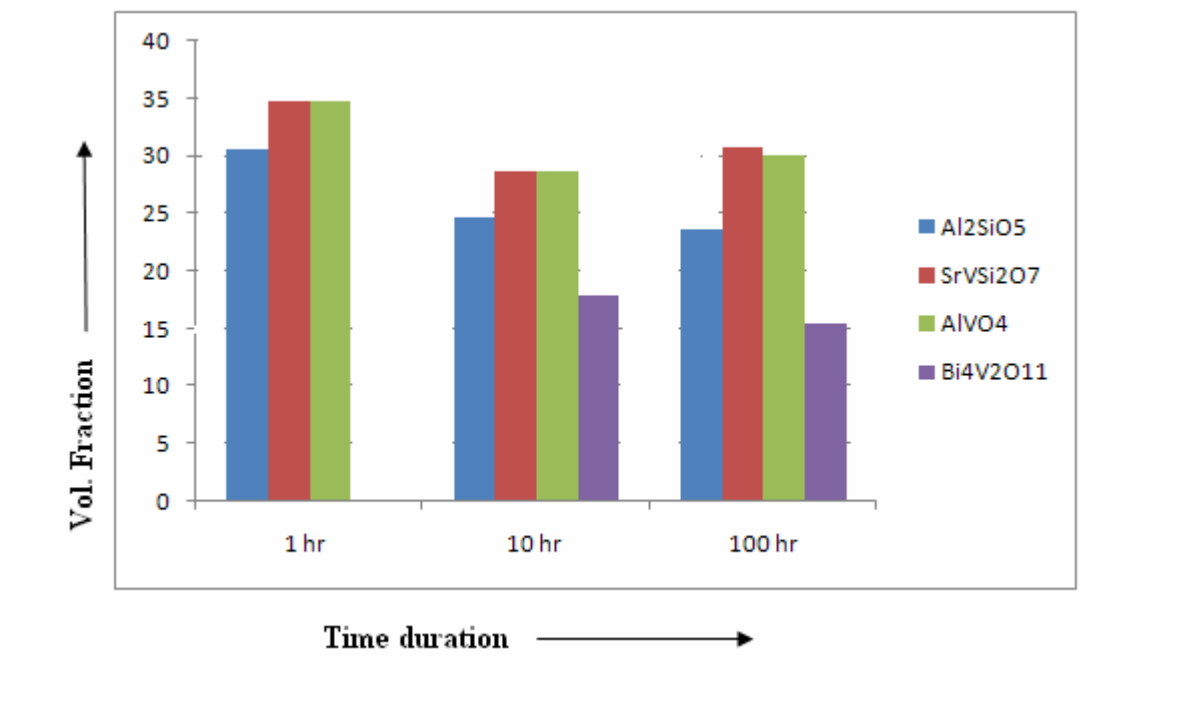

Fig 5.7: Variation of volume fraction of phases with increase in time duration of heat treatment for IS3 sample.

Table 5.4: Crystalline phases and their volume fraction with different heat treatment durations for sample IS4:

Time duration(hr)	Volume fraction the phases (%)			
	$Cr_2(SiO_4)$	$SrVSi_2O_7$	$CrVO_4$	$Bi_4V_2O_{11}$
10	22.37	32.89	22.37	22.37
100	25.51	25.51	24.48	24.48

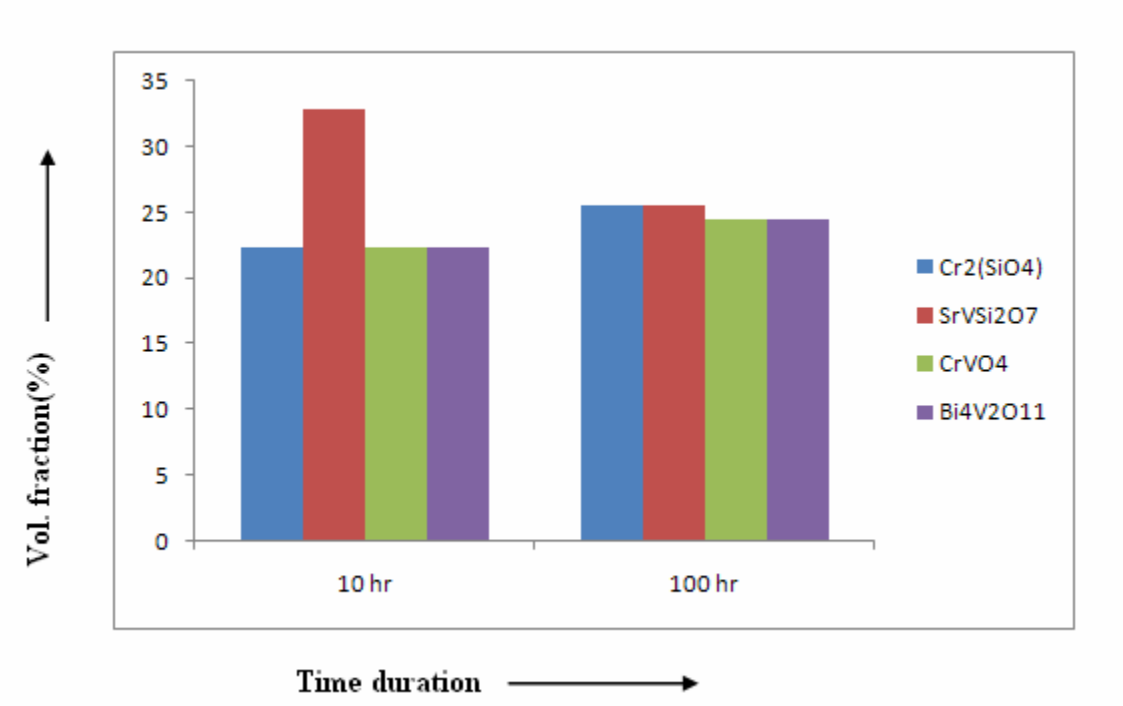

Fig 5.8: Variation of volume fraction of phases with increase in time duration of heat treatment for IS4 sample

XRD pattern of the sample IS1 are given in the figure 5.1 for 1 hr, 10 hrs and 100 hrs heat treatment. The volume fractions of different phases with heat treatment duration of the same sample are shown in figure 5.5. The XRD results show the formation of phases Y_2SiO_5, $SrVSi_2O_7$, YVO_4 and $Bi_{12}V_2O_{23}$ phases. After 1 hr heat treatment the sample exhibit mainly $SrVSi_2O_7$, Y_2SiO_5 and YVO_4. As the time duration of heat treatment progresses the volume fraction of $SrVSi_2O_7$ phase decreases. However, the volume fraction of Y_2SiO_5 phase increases. It means volume fraction of Y_2SiO_5 phase increases on the expense of $SrVSi_2O_7$ due to high field strength of Y^{+3} [29 & 30] it attracts silicate tetrahedron which breaks bond with Sr and V and bond with Y to form Y_2SiO_5. While the YVO_4 and $Bi_{12}V_2O_{23}$ phases almost remain constant with increasing heat treatment durations.

For the sample IS2 XRD pattern are given in the figure 5.2 for 1 hr, 10 hrs and 100 hrs heat treatment. The XRD results show the formation of phases La_2SiO_5, $SrVSi_2O_7$, $LaVO_4$ and $BiVO_4$. $LaVO_4$ is the phase which is prominent during all heat treatments whereas the volume fraction of the $SrVSi_2O_7$ phase increases with time and La_2SiO_5 decreases with time because field strength of La^{+3} is less than Y^{+3} [30] due to this La_2SiO_5 disintegrate with time and SiO_4 tetrahedron combines with $SrVSi_2O_7$ and the volume fraction of $SrVSi_2O_7$ increases and La combines with V to form $LaVO_4$ whose volume fraction increases from 10 to 100 hrs. The volume fraction of the $BiVO_4$ remains almost same with minor variation as shown in figure 5.6.

XRD pattern of the sample IS3 are given in the figure 5.3 for different heat treatment durations. The XRD patterns of IS3 sample exhibits Al_2SiO_5, $SrVSi_2O_7$, $AlVO_4$ and $Bi_4V_2O_{11}$ phases which were identified using powder diffraction files (PDF). Initially this particular sample exhibit only three phases i, e Al_2SiO_5, $SrVSi_2O_7$ and $AlVO_4$. As the heat treatment progresses, phase $Bi_4V_2O_{11}$ is also formed and its volume fraction do not changes with further heat treatment and the major phase in 1 hr heat treatment Al_2SiO_5 and $AlVO_4$ are having triclinic crystal structure which is most unstable which results in decrease in the volume fraction with further increase in heat treatment duration as shown in figure 5.7. On the other hand, $SrVSi_2O_7$ remains almost constant up to 100 hrs heat treatment.

In the case of sample IS4, after 1 hr heat treatment, the sample did not show the crystallization. As the heat treatment duration increases different crystalline phases are formed as shown in figure 5.8. These phases are $Cr_2(SiO_4)$, $SrVSi_2O_7$, $CrVO_4$ and γ - $Bi_4V_2O_{11}$. The volume fraction with respect to heat treatment duration is depicted in figure 5.8. $SrVSi_2O_7$ phase decreases with increasing heat treatment time duration. All the other phases could not show appreciable change in their volume fraction. $SrVSi_2O_7$ being orthorhombic is more stable so this phase is preferentially formed. However, Cr being more reactive leads to increase in volume fraction of Cr_2SiO_4 and $CrVO_4$ at the expense of $SrVSi_2O_7$ [28].

In all the four samples, $SrVSi_2O_7$ phase is prominent and $SrVSi_2O_7$ being orthorhombic is more stable so this phase is preferentially formed its volume fraction decreases with progressive heat treatment durations except in case of IS2 sample where La_2O_3 is used as a glass modifier . It clearly indicates that the activation energy of this phase is lesser than other formed phase. Apart from this, this phase might be less symmetric than other phase. However the anomaly was observed in case of IS2 sample. This might be attributed that La^{+3} increases the reaction between Sr^{+2}, Si^{+4} and V^{+5} species of $SrVSi_2O_7$ phase. La^{+3} show higher affinities with Si and V in all the four samples. Interesting Cr^{+3}exhibit lower affinity with Si and V.

5.2 FTIR Analysis

Infrared spectra photometry was carried out on all samples to identify the functional groups present in these samples. In the spectra shown in figures 5.9 to 5.12 some of the peaks in the higher wave number region are due to the acetone group and others due to water molecules which have been used during sample preparation. The main peaks are due to silicate groups which are present in higher mol% in the sample. The FTIR spectra of all the samples which are heat treated at 800° C for 1 hr, 10 hr and 100 hrs are given in this section.

Generally, alkaline earth oxides (MgO, BaO, CaO, SrO) will not show any band in the IR spectra of silicate glasses. However, they will shift the bands (especially, in the region 800-1300 cm^{-1}) towards higher or lower wave numbers. This shift in bands towards lower or higher wave numbers depicts the connectivity in the glass structure (number of bridging oxygen, Q1, Q2…etc) [29]. The FTIR region from 400-1300 cm^{-1} is generally divided into three main regions for alumino silicate glasses [28, 30]. One of the transmissions band regions is from 400-600 cm^{-1} and in this region the linkages are due to Si-O-Si and Si-O- A (A=Al, Cr, Y, La) linkages. Another transmission region is from 650- 800 cm^{-1} [28, 30] and the bonding in this region is due to A-O (A= Al, Cr, Y, La) linkages. The third one transmission region is from 800- 1300 cm^{-1}[30] and the bonding in this region is due to stretching vibration of SiO_4 tetrahedron.

If boron is present boron in silicate glasses, in general it shows three bands [31].

a) 600-800 cm^{-1} b) Around 1000cm^{-1} c) 1300-1500cm^{-1}.

Generally, in silicate glasses, band (b) is overlapped by the band of SiO_4 in the region 800-1300 cm^{-1}. So, it is difficult to observe the same in borosilicate glasses. Similarly, presence of Al_2O_3 in a borosilicate glass shows a band in the region 650-800cm^{-1}, which overlaps band (a). These two bands play their role in modifying the structure of glass. The third band in the region 1300-1500 cm^{-1} is generally observed for boron [32].

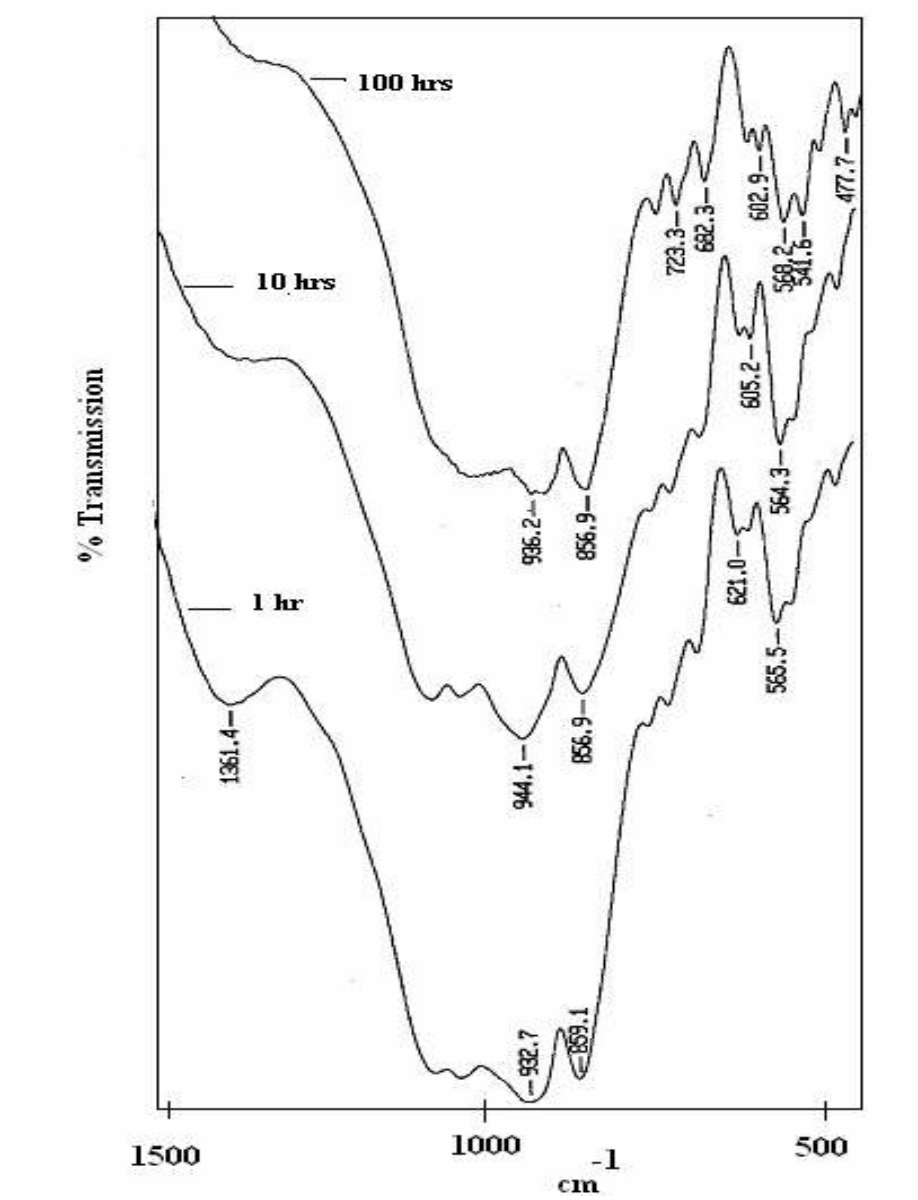

Fig 5.9 FTIR transmission spectra of the IS1 sample heat treated for 1 hr, 10 hr and 100 hrs

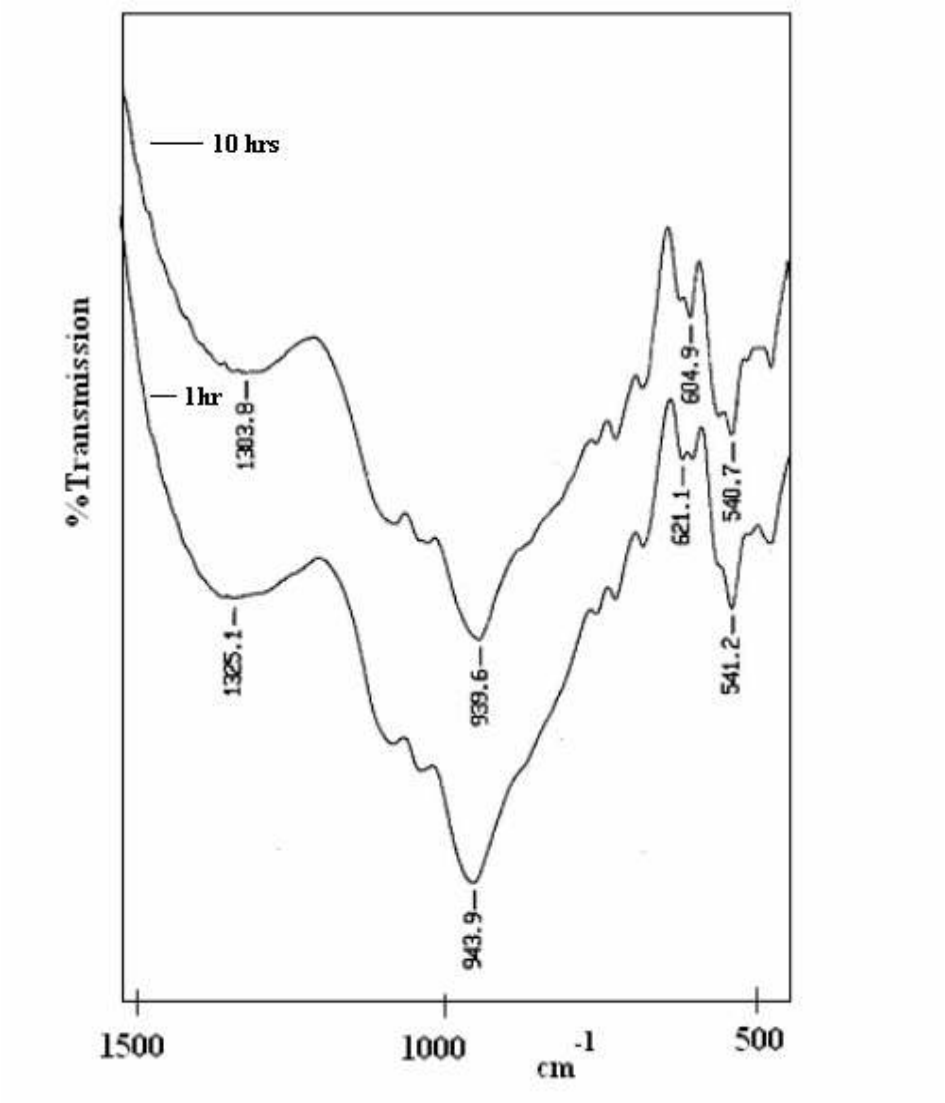

Fig 5.10 FTIR transmission spectra of the IS2 sample heat treated for 1 hr and 10 hrs

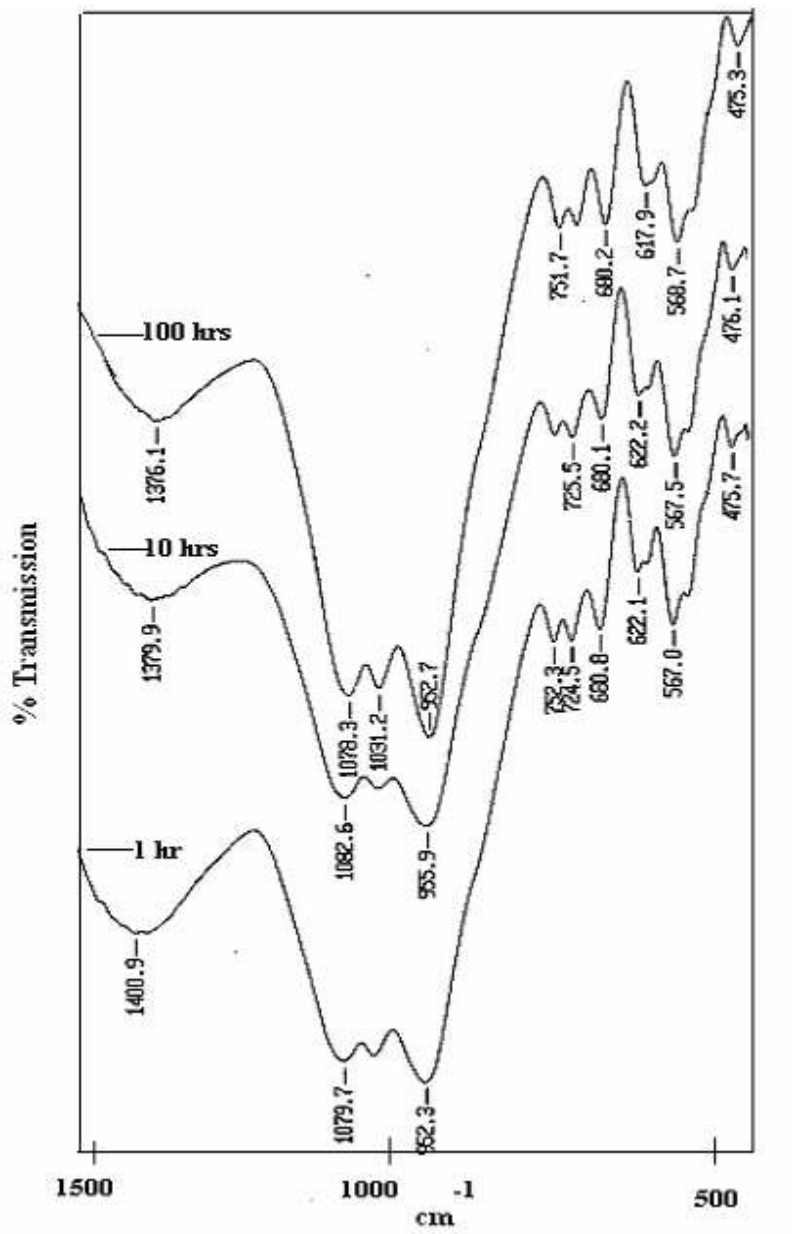

Fig 5.11 FTIR transmission spectra of the IS3 sample heat treated for 1 hr, 10 hr and 100 hrs

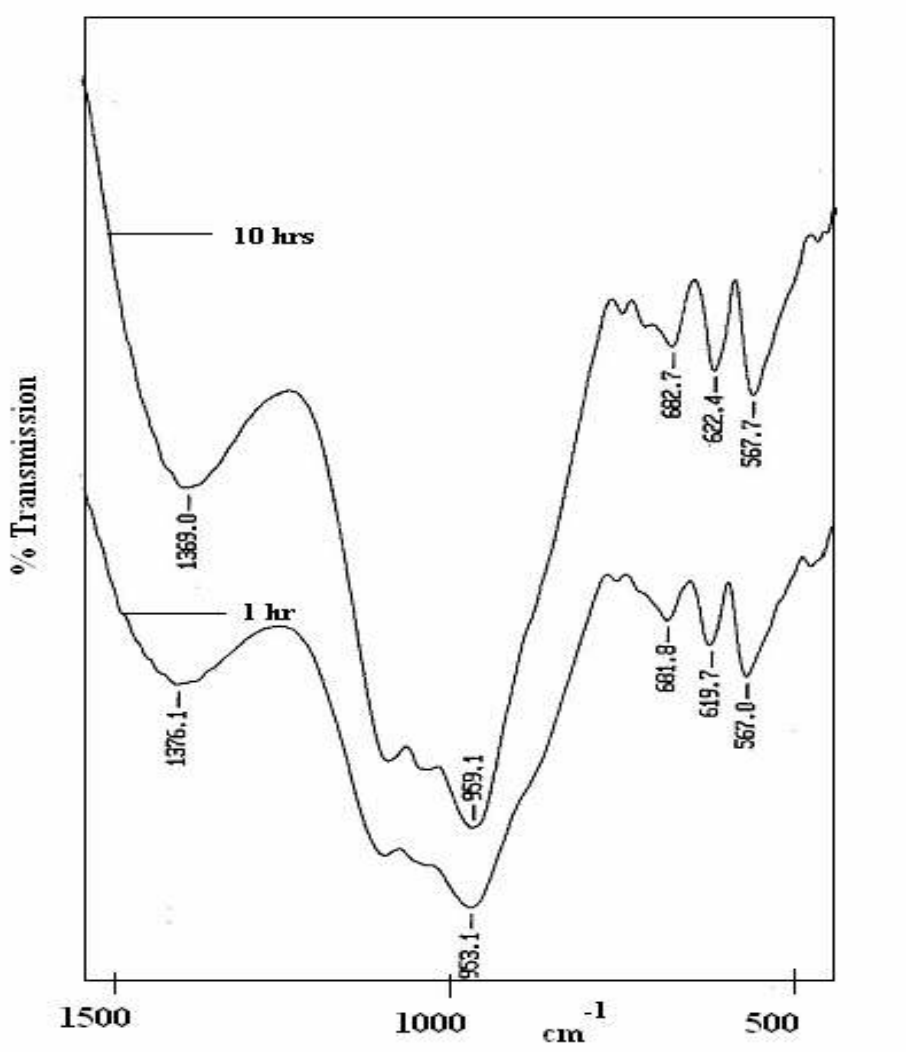

Fig 5.12 FTIR transmission spectra of the IS4 sample heat treated for 1 hr and 10 hrs

FTIR Spectra for the samples IS1, IS2, IS3 and IS4 for 1 hr, 10 hrs and 100 hrs heat treatments are given in figures from 5.9 to 5.12. These spectra are generally divided into three regions from 400-600 cm^{-1}, 650-800 cm^{-1} and 800-1300 cm^{-1}. The first transmission region is due to the bending vibrations of the Si-0-Si and Si-O-A (A=Y, La, Al and Cr) linkages. The second region can be assigned to bending vibrations of the A-O (A= Y, La, Al and Cr) bonds with A^{+3} ions in the four- fold coordination [30]. The third region peaks are assigned to the stretching vibrations of the SiO_4 tetrahedron with the different numbers of bridging oxygen atoms [30]. There is a little bit shifting of peaks to lower wave number suggesting some structural rearrangement in silicate glass network due to heat treatment [28] and presence of B_2O_3 [32].

The FTIR spectra of IS1 are shown in figure 5.9. There are three transmission band regions as described above and for the first region from 400-600 cm^{-1} there is continuous decrease in the intensity of the peaks as the time duration of heat treatment increases from 1 hr to 10 hrs and then from 10 hrs to 100 hrs as described above the peaks in this region are due to the bending vibrations of the Si-0-Si and Si-O-Y centered around 565 showing continuous decrease in the volume fraction of the phase $SrVSi_2O_7$ where Si-O-Si linkages are present. While the another region from 800-1300 cm^{-1} which is due to the stretching vibrations of the SiO_4 tetrahedron present in Y_2SiO_5 phase whose volume fraction increases with increase in time duration of heat treatment. A little deviation of FTIR spectra after 100 hrs heat treatment signifies occurrence of some rearrangement in network structure [30]. There is a broad peak at 1361 cm^{-1} after 1 hr heat treatment which might correspond to B-O vibrations in [BO3] triangle and is clear from the spectra that this peak almost flattens as the time duration of heat treatment increase [31 ,32]. The region 650- 800 cm^{-1} is the weak intensity region is having bending vibrations of Y-O bond almost centered around 723 cm^{-1} whose peak intensity increases with time.

The FTIR spectra of the IS2 shown in figure 5.10 the region from 400-600 cm^{-1} signifies the bending vibrations of the Si-0-Si and Si-O-La centered around 540 cm^{-1} due to $SrVSi_2O_7$ and La_2SiO_5 phases respectively. The region from 600-850 cm^{-1} where Si- O^- stretching with two

non-bridging oxygen is present there is little bit of decrease in peak intensity from 1 hr heat treatment to 10 hrs. The peak center is observed at 605 cm^{-1}. A peak is observed at 943.9 cm^{-1} in 1 hr heat treatment. This peak might be attributed to BO_4 stretching [31, 32] which shifts to lower wave number with increased intensity as time duration for heat treatment increases. There is another peak at 1303 cm^{-1} after 1 hr heat treatment which might correspond to B-O vibrations in [BO_3] triangle and intensity of this peak increases as the time duration of heat treatment increases [31].

In case of IS3 sample the intensity in region from 400-600 cm^{-1} decreases as the time duration of heat treatment increases from 1 hr to 10 hrs. However, the intensity could not change from 10 hrs to 100 hrs heat treatment. As described above the peaks in this region are due to the bending vibrations of the Si-0-Si and Si-O-Al centered on 475 cm^{-1} and 567 cm^{-1}. While the region 800-1300 cm^{-1} corresponds to stretching vibrations of the SiO_4 tetrahedron in Al_2SiO_5 there is decrease in the peak intensity as the time duration for heat treatment increases i.e Al_2SiO_5 decreases with increase in time duration of heat treatment. The third region from 650-800 cm^{-1} is due to stretching vibration of Al-O bonds in $AlVO_4$ with Al^{+3} ions is in fourfold co-ordination[30]. There is a broad peak at 1400 cm^{-1} after 1 hr heat treatment and this peak broadened as the time duration for heat treatment progresses and are due to the B-O vibrations in [BO_3] triangle and shift towards lower wave numbers as the time duration for heat treatment progresses suggesting some structural rearrangement in alumino-silicate network structure [28]. Some peaks are also observed in the higher wave number regions and are due to water or acetone as shown in figure 5.11.

FTIR spectra of the IS4 sample is shown in figure 5.12. A band is observed in the region from 400-600 cm^{-1}, corresponds to the bending vibrations of the Si-0-Si. The transmission intensity of the peaks decreases as the time duration of heat treatment increases from 1 hr to 10 hrs. Another region from 800- 1300 cm^{-1} is correspond to the stretching vibrations of the SiO_4 tetrahedron in Cr_2SiO_4 there is decrease in the transmission peak intensity as the time duration for heat treatment increases similar results are also observed by A. Aronne [30] . The peak positions and observed infra red absorption bands are given in table 5.5

Table 5.5 Positions and assignment of the observed infrared absorption bands [31]:

Peak position (cm^{-1})	**Assignment**
Silicate chain	
1065–1095	Si–O–Si anti-symmetric stretching of bridging oxygen within the tetrahedral
940–970	$Si–O^-$ stretching with one non-bridging oxygen
860–940	$Si–O^-$ stretching with two non-bridging oxygens
750–820	Si–O–Si symmetric stretching of bridging oxygen
460–510, 600	Si–O–Si and O–Si–O bending modes (V4
Borate chains	
(a) BO_3 stretching	
1420–1550	B–O bonds vibrations
1550–1400	B–O vibrations of various borate groups
1250	Boroxol rings, tri-, tetra- and pentaborate groups pyro- and other borates
1220–1250	

(b) BO_4 stretching	
1050	Tri-, tetra-, and pentaborate
900–1000	Diborate
880	Tri-, tetra and penta-borate oxygen bridges between tetra- and trigonal boron
760–770	
690–730	atoms oxygen bridges between trigonal atoms
Other groups	
1640	Molecular water
1460	Carbonate group
3000–3750	Hydrogen, molecular water, silanol group (SiOH)
650-800	Al- O stretching vibrations

5.3 Thermal Expansion Coefficient

In order to determine the thermal compatibility of the glass sealant with Bismuth Vanadate, the thermal expansion coefficient of IS2 sample was determined by dilatometer in the temperature range of 100-650°C. Apart from this, the TEC of virgin glass (S2) and electrolyte were also determined. A typical TEC plot of IS2 sample is shown in figure 5.13. The data of TEC are given in table5.6. The TEC values of all the three samples are very close to each other. The TEC values are also matching with the desired value of other components of SOFC i ,e. 8-11 X 10^{-6}/°C.**Table 5.6:** TEC value of glass, electrolyte and coupled glass- electrolyte samples

Sample name	**TEC (X 10^{-6}/°C)**
S2	7.75
Electrolyte	8.15
IS2	8.02

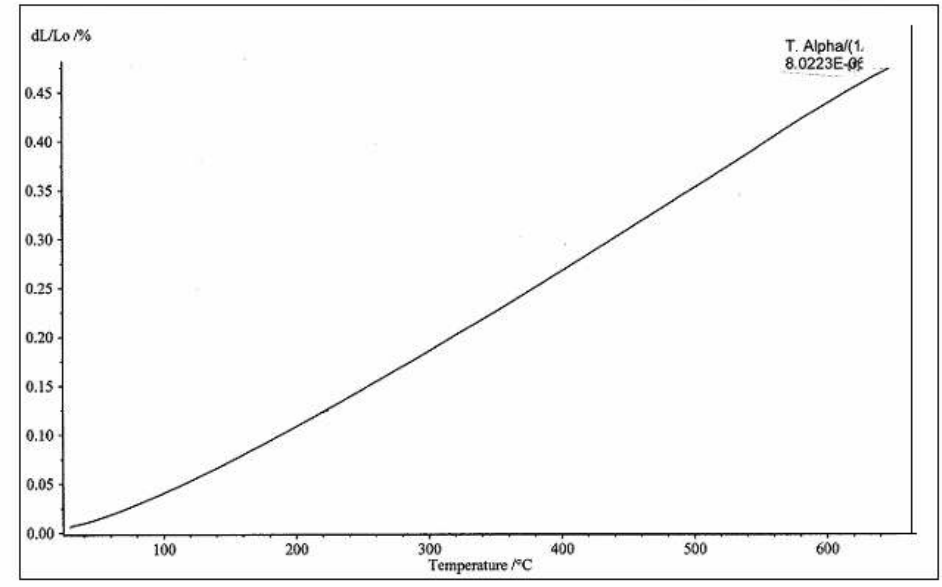

Fig 5.13: Dilatometry plot for IS2

CHAPTER-6

CONCLUSION AND FUTURE ASPECT

The interaction study of glass sealants and with other components of SOFC's is very important in planar SOFC. For longer working of planar SOFC there should be minimum rather no detrimental phase interaction between the various components of SOFC and glass sealants. To maintain the structural stability and to minimize the degradation and/or failure of SOFC stack performance, the sealing glass should have chemical compatibility with the interconnector and PEN (Positive electrode- electrolyte-negative electrode). If there is any type of interaction between glass sealant and components then it is important to determine which type of phases are forming or whether the formed phase is harmful for SOFC or either having TEC matching or not.

The chemical interactions among glass sealants and $Bi_4V_{1.8}Al_{0.2}O_{11}$ electrolyte are studied. The glass and electrolyte are taken in ratio 3:1 wt%, respectively. Mixture of these components were heat treated for different time durations and then characterized by X-ray diffraction (XRD), Fourier Transform Infra Red spectroscopy (FTIR) and dilatometer to determine the possible reaction phases, their volume fraction and prominent IR band formation. The main conclusions drawn from study are:

1. In interaction study, the major phases $SrVSi_2O_7$, AVO_4, A_2SiO_5 (A= Y, La, Al, Cr) were formed.
2. The change in volume fraction of these phases with heat treatment duration depends on various factors such as ionic radii, their affinity to each other, and field strength of the cations.
3. The FTIR spectra of all the samples exhibit three bands i,e 400-600 cm^{-1}, 650-800 cm^{-1} and 800- 1300 cm^{-1} . These spectra are assigned to bending vibrations of the Si-0-Si linkages, bending vibrations of the A-O (A= Y, La, Al and Cr) bonds and stretching vibrations of the SiO_4 tetrahedron with the different numbers of bridging oxygen atoms.

4. The thermal expansion coefficient of diffusion couple (electrolyte and glass) is 8 $X10^{-6}/°C$ which is very close to required value of SOFC components.

Future Scope:

In order to understand the stability and long term behavior of the various phases the powder mixture of these samples will be heat treated for longer duration so that crystallization kinetics of phases will be understood properly. SEM can be carried to study the morphological characters of the detrimental phases which have been indexed by XRD results.

REFERENCES:-

[1] R. Mark Ormerod, Chem. Soc. Rev., 2003, 32, 17–28.

[2] Carrette, L.; Friedrich, K, A.; Stimming, U. ChemPhysChem 2000,1, 162.

[3] S. C. Singhal, "Science and Technology of Solid-Oxide Fuel Cells," MRS Bull. Vol.25, No.3, 2000, p.16-21.

[4] Timo Kivisaari, S.Thyberg Naumann, O.Lindstrom, and P.Bjornbom, Az, 1992, pp. 329-331.

[5] A.D Hawkes, L Exarchakos, D Hart, MA Leach, Ir. D. Haeseldonckx, Ir. L. Cosijns, Prof. Dr. Ir. W. D'haeseleer" an introduction to fuel cells

[6] Qingfeng Li, Ronghuan He, Jens Oluf Jensen, and Niels J. Bjerrum, Chem. Mater., 15 (26), 4896 -4915, 2003.

[7] Matthew M Mench, Chao-Yang and Stefan T. Thynall " an introduction to fuel cells and transport phenomena" ,electrochemical centre.

[8] S.C. Singhal , science and technology of solid oxide fuell cells MRS Bulletin/march 2000, p 16-21.

[9] Ivers-Tiffee, E., Weber, A., and Herbstritt, D. (2001). "Materials and technologies for SOFC-components." Journal of the European Ceramic Society, 21(10-11), 1805-1811.

[10] S.C.Singhal, Solid State Ionics 135 (2000), 305–313.

[11] S.M. Gross, T. Koppitz, N.H. Menzler, American Ceramics Society, 2006 209-217.

[12] Jun-Young Park . Eric D. Wachsman, Ionics (2006) 12: 15–20

[13] F. Krok, I. Abrahams, W. Wrobal, A. Kozanecka-Szmigiel, J.R.Dygas, Materials Science-Poland, Vol. 24, No. 1, 2006.

[14] R. Kant, K. Singh, O.P. Pandey, "Effect of Ti_2O_3 substitution in Bismuth Vanadate Electrolyte" Accepted in Indian Ceramics Society (2007).

[15] R vanadate electrolyte material with aluminum doping for SOFC applications" Ceramics International (2007), in press.. Kant, K. Singh, O.P. Pandey, "Synthesis and characterization of bismuth

[16] K. Scott Weil, John S. Hardy, and Brian J. Koeppel, ASM International,Volume 15(4) August 2006-427.

[17] J.W. Fergus / Journal of Power Sources xxx (2005) xxx–xxx

[18] K. Scott Weil , JOM 2006 p (37-44)..

[19] D. Bahadur, N. Lahl, K. Singh, L. Singheiser, and K. Hilpertz, Journal of The) Electrochemical Society, 151 (4) A558-A562 (2004).

[20] Zhenguo Yang, Guanguang Xia, Kerry D. Meinharat, ASM International, vol 13(3) June 2004-327

[21] Apichart Jinnapat, Sirithan Jiamsirilert and Sumittra Charojrochkul,journal of material online June-2007, vol 3 (1-8).

[22] Sung-Bum Sohn and Se-Young Choi, J. Am. Ceram. Soc., 87 [2] 254–60 (2004).

[23] Ashutosh Goel, Dilshat U. Tulyaganov,z Vladislav V. Kharton, Aleksey A. Yaremchenko, Simeon Agathopoulos,,y and Jose´ M. F. Ferreira, J. Am. Ceram. Soc., 90 [7] 2236–2244 (2007)

[24] N. Lahl, D. Bahadur, K. Singh, L. Singheiser, and K. Hilpertz, Journal of The Electrochemical Society, 149 (5) A607-A614 (2002).

[25] Yi- Ju Chen, W. C. W, The Suitability of BaO-B2O3-SiO2-Al2O3 Glass System Used as Sealants for Solid Oxide Fuel Cell

[26] Kerry Meinhardt, Dong-Sang Kim,Gary Yang, Matt Chou" glass sealing of solid oxide fuel cells", ceramics2007.

[27] R. Kant, K. Singh, O.P. Pandey, "Micro structural and Electrical behavior of Cu-substituted $Bi4V2_{-x}Me_x O_{11-\delta}$ ($0 \le x \le 0.4$)" Accepted in Ceramics International (2007), in press.

[28] A. Goel , Dilshat U. Tulyaganov , V. Kharton "The effect of Cr_2O_3 addition on crystallization and properties of La2O3-containing diopside glass-ceramics",Acta Materialia(2008)

[29] K .Singh, N. Gupta, O .P. Pandey," effect of Y2O3 on the crystallization behaviour of SiO_2-MgO-B_2O_3-Al_2O_3 glasses", J Mater Sci (2007).

[30] A. Aronne , S. Esposito, P. Pernice "FTIR and DTA study of lanthanum aluminosilicate glasses " , Material Chemistry and Physics (1997).

[31] Fatma H.A. Elbatal , Magda M.I. Khalil "Gamma rays interaction with ternary silicate glasses containing mixed CoO + NiO" , Material Chemistry and Physics (2003).

[32] A. Goel , Dilshat U. Tulyaganov F. Ferreira " effect of BaO on the crystallization kinetics of glasses along the diopside –Ca Tschermak join" (2008).